AD ________________

MIPR NUMBER 96MM6785

TITLE: The Cytoskeleton and ATP in Sulfur Mustard-Medicated Injury to Endothelial Cells and Keratinocytes

PRINCIPAL INVESTIGATOR: Daniel B. Hinshaw, M.D.

CONTRACTING ORGANIZATION: Department of Veterans Affairs
Medical Center
Ann Arbor, Michigan 48105

REPORT DATE: July 1998

TYPE OF REPORT: Midterm

PREPARED FOR: Commander
U.S. Army Medical Research and Materiel Command
Fort Detrick, Frederick, Maryland 21702-5012

DISTRIBUTION STATEMENT: Approved for public release;
distribution unlimited

The views, opinions and/or findings contained in this report are those of the author(s) and should not be construed as an official Department of the Army position, policy or decision unless so designated by other documentation.

20000609 056

DTIC QUALITY INSPECTED 4

REPORT DOCUMENTATION PAGE

Form Approved
OMB No. 0704-0188

Public reporting burden for this collection of information is estimated to average 1 hour per response, including the time for reviewing instructions, searching existing data sources, gathering and maintaining the data needed, and completing and reviewing the collection of information. Send comments regarding this burden estimate or any other aspect of this collection of information, including suggestions for reducing this burden, to Washington Headquarters Services, Directorate for Information Operations and Reports, 1215 Jefferson Davis Highway, Suite 1204, Arlington, VA 22202-4302, and to the Office of Management and Budget, Paperwork Reduction Project (0704-0188), Washington, DC 20503.

1. AGENCY USE ONLY *(Leave blank)*

2. REPORT DATE
July 1998

3. REPORT TYPE AND DATES COVERED
Midterm (1 Oct 96 - 31 May 98)

4. TITLE AND SUBTITLE
The Cytoskeleton and ATP in Sulfur Mustard-Medicated
Injury to Endothelial Cells and Keratinocytes

5. FUNDING NUMBERS
96MM6785

6. AUTHOR(S)
Daniel B. Hinshaw, M.D.

7. PERFORMING ORGANIZATION NAME(S) AND ADDRESS(ES)
Department of Veterans Affairs Medical Center
Ann Arbor, Michigan 48105

8. PERFORMING ORGANIZATION REPORT NUMBER

9. SPONSORING/MONITORING AGENCY NAME(S) AND ADDRESS(ES)
Commander
U.S. Army Medical Research and Materiel Command
Fort Detrick, Frederick, Maryland 21702-5012

10. SPONSORING/MONITORING AGENCY REPORT NUMBER

11. SUPPLEMENTARY NOTES

12a. DISTRIBUTION / AVAILABILITY STATEMENT

Approved for public release; distribution unlimited

12b. DISTRIBUTION CODE

13. ABSTRACT *(Maximum 200*

The major goal of this project is to test the hypothesis that sulfur mustard (SM)-mediated cell death in keratinocytes and endothelial cells is primarily apoptotic in nature, and that several factors (e.g., cellular levels of adenosine triphosphate (ATP), reactive oxygen species [ROS]) help define this process. Using biochemical and fluorescence microscopic techniques to measure several parameters of cell death over a 72 hour time course of SM injury, we found that keratinocytes develop mixed features of both apoptosis and necrosis, but more slowly than endothelial cells which exhibit a more classical pattern of apoptosis. Caspase-3, a protease which plays a central role in programmed cell death was activated in both cell types by SM. In a model of moderate ATP depletion (~50% of control) endothelial cell progression into apoptosis was suppressed after SM injury followed by later increases in necrosis at higher SM concentrations. Protective effects of N-acetyl-l-cysteine (NAC) on SM-injured endothelial cells were found to be glutathione (GSH)-dependent but other studies assaying for ROS within SM-injured cells were as yet inconclusive. Our results thus far suggest that cell death induced by SM may represent a continuum between the extremes of apoptosis and necrosis. Caspase activation appears to be a critical element common to SM-induced endothelial cell and keratinocyte death and thus may be an important target for therapeutic intervention.

14. SUBJECT TERMS
sulfur mustard, keratinocytes, endothelium, microfilaments,
actin, apoptosis, cell death

15. NUMBER OF PAGES
81

16. PRICE CODE

17. SECURITY CLASSIFICATION OF REPORT	18. SECURITY CLASSIFICATION OF THIS PAGE	19. SECURITY CLASSIFICATION OF ABSTRACT	20. LIMITATION OF ABSTRACT
Unclassified	Unclassified	Unclassified	Unlimited

FOREWORD

Opinions, interpretations, conclusions and recommendations are those of the author and are not necessarily endorsed by the U.S. Army.

____ Where copyrighted material is quoted, permission has been obtained to use such material.

____ Where material from documents designated for limited distribution is quoted, permission has been obtained to use the material.

DSM Citations of commercial organizations and trade names in this report do not constitute an official Department of Army endorsement or approval of the products or services of these organizations.

____ In conducting research using animals, the investigator(s) adhered to the "Guide for the Care and Use of Laboratory Animals," prepared by the Committee on Care and Use of Laboratory Animals of the Institute of Laboratory Resources, National Research Council (NIH Publication No. 86-23, Revised 1985).

____ For the protection of human subjects, the investigator(s) adhered to policies of applicable Federal Law 45 CFR 46.

____ In conducting research utilizing recombinant DNA technology, the investigator(s) adhered to current guidelines promulgated by the National Institutes of Health.

____ In the conduct of research utilizing recombinant DNA, the investigator(s) adhered to the NIH Guidelines for Research Involving Recombinant DNA Molecules.

____ In the conduct of research involving hazardous organisms, the investigator(s) adhered to the CDC-NIH Guide for Biosafety in Microbiological and Biomedical Laboratories.

7/24/98
PI - Signature Date

TABLE OF CONTENTS

Mid-Term Report Front Cover 1

Report Documentation Page 2

Foreword 3

Table of Contents 4

Introduction 5

Body 8

  Experimental Methods, Assumptions, and Procedure 8

  Results 18

  Discussion 28

  Conclusions 32

References 33

Figure Legends 38

Tables 41

Figures 47

INTRODUCTION

The chemical warfare vesicant, sulfur mustard (SM), continues to be an effective weapon of terror eighty years after the end of World War I. Largely because of an incomplete understanding of the pathogenesis of SM-induced vesication, no effective therapy currently exists for SM. The primary focus of this project is to test the hypothesis that SM induces programmed cell death or apoptosis in endothelial cells and keratinocytes, two major cellular targets intimately involved in the vesication process. It is further hypothesized that the morphologic and cytoskeletal alterations in SM-injured endothelial cells and keratinocytes are largely apoptotic in character, SM-induced apoptosis is an ATP-dependent process, and reactive oxygen species (ROS) generated within SM-injured cells may act as initiating signals for apoptosis. This mid-term report will present progress we have made in addressing these questions, specifically addressing work proposed in tasks 1-7 of the Statement of Work (SOW).

The process of cell death usually follows one of two patterns: necrosis or apoptosis (programmed cell death) (1-4). Necrosis, typically, has been seen as an "accidental" or catastrophic form of cell death, characterized by cellular swelling and loss of plasma membrane integrity. Apoptosis, in contrast, is a highly coordinated form of cellular "suicide", the hallmark of which has been a morphologic pattern of nuclear chromatin condensation and fragmentation associated with cell shrinkage, membrane budding (blebbing), and ultimate fragmentation of the cell and chromatin into many smaller membrane-enclosed apoptotic bodies. The apoptotic bodies retain intact plasma membranes for some time and *in vivo* are phagocytized by neighboring cells or macrophages (1-4). Apoptosis is thought to occur "silently" with little or no acute inflammation, whereas necrosis usually evokes a prominent acute inflammatory response (1). A wide variety of stimuli can induce the apoptotic process, including physiologic (e.g. normal development, steroid hormones, removal of trophic factors) and pathologic stimuli (e.g. ischemia, oxidants, adverse physical conditions such as hypothermia, chemotherapeutic agents for cancer, and agents which disrupt the cytoskeleton). Many of the pathologic agents which induce apoptosis at low concentrations in a given cell will cause necrosis in the same cell at higher concentrations (1). This appears to also be true for SM (5). Concentrations of SM which alter cellular metabolism (e.g. reduce cellular ATP levels) can induce necrosis in endothelial cells (5). In contrast, a number of laboratories have recently demonstrated the ATP-dependence of apoptosis, underscoring the importance of intact metabolic pathways for successful implementation of the death program of apoptosis (6-10).

Recent advances in understanding the biochemical pathways of apoptosis have led to the identification of two major phases in apoptosis: a potentially reversible initiation phase and a later irreversible execution phase (4). A central component to the apoptotic process is the activity of a family of cysteine proteases known as the caspases (4,11,12). The caspases have been referred to as the "central executioner" of apoptosis (4) because it is thought that they catalyze activity marking the "point of no return" in apoptosis leading to the final events of the execution phase (e.g. nuclear fragmentation and endonucleolytic cleavage of DNA, plasma membrane phospholipid changes, and actin filament depolymerization and actin cleavage).

Although in many cells apoptosis and necrosis appear to be fairly distinct, even mutually exclusive, pathways of cell death, such sharp distinctions do not always exist -

even apoptotic cells eventually lose plasma membrane integrity (if they do not undergo phagocytosis) and not all of the individual features of apoptosis (e.g. endonucleolytic cleavage of DNA) may occur in a given cell type or following a particular apoptotic stimulus. In recent work we reported that endothelial cells demonstrate a number of classical features of apoptosis (including nuclear chromatin condensation and fragmentation, endonucleolytic cleavage of DNA, cellular shrinkage, membrane budding, actin filament depolymerization, and apoptotic body formation and release) following exposure to SM (5). In preliminary work presented in our last contract's final report, keratinocytes appeared to undergo necrosis almost exclusively after SM exposure as measured by loss of plasma membrane integrity, and demonstrated little evidence of the apoptotic changes in nuclear chromatin typically seen in SM-injured endothelial cells. Rosenthal, et. al. have reported recently that cleavage of poly (ADP-ribose) polymerase (PARP) by caspase-3, an event central to the apoptotic process, does occur in SM-injured keratinocytes (13). In other models of keratinocyte injury and death, some if not many features of apoptosis (including evidence of nuclear degradation and endonucleolytic cleavage of DNA) have been demonstrated (14-16). These observations coupled with our earlier observations of plasma membrane lysis in keratinocytes following SM exposure suggest that the distinction between apoptosis and necrosis may not be clear-cut. Furthermore, the minimal essential elements that characterize programmed cell death as a distinct entity (particularly with respect to keratinocyte injury by SM) have not been defined, although Smulson and Rosenthal suggest that caspase activation may indeed be the all sufficient and defining event required for the process (13).

The report which follows details our progress to date in addressing the work outlined in the SOW and our effort to examine in more detail many of the unique features which characterize keratinocyte and endothelial cell death induced by SM.

BODY

EXPERIMENTAL METHODS, ASSUMPTIONS, AND PROCEDURES.

Cells and culture. Bovine pulmonary artery endothelial cells were purchased from the National Institute of Aging, Aging Cell Culture Repository (Camden, NJ) and maintained in Ham's F12 medium supplemented with 2 mM glutamine (GIBCO), 10% heat-inactivated fetal bovine serum (GIBCO), 10 mM HEPES, 100 U/ml penicillin, and 100 mg/ml streptomycin (GIBCO). Endothelial subculturing was carried out on confluent cultures using 0.05% trypsin and 0.02% EDTA (Sigma) and cells of Passages 3 to 9 were used. Human keratinocytes from redundant skin removed at the time of reduction mammoplasty (courtesy of Dr. Cynthia Marcelo, University of Michigan) were grown in KBM-2 medium (Clonetics) with the addition of growth factors (KGM-2 single quots, Clonetics). Upon reaching 80% confluence, the keratinocytes were passaged by exposure to 0.05% trypsin and 0.02% EDTA. The trypsin was inactivated with 10-15 ml of 0.3 mg/ml soybean trypsin inhibitor (Clonetics). Keratinocytes from the first to third passages were used for experiments. Cells were grown in 75- or 150-cm^2 flasks (Falcon) in a culture incubator at 37°C under a 5% CO_2 humidified atmosphere.

Injury protocol with SM. Confluent monolayers of endothelial cells or keratinocytes grown in six-well plates (Falcon, Becton Dickinson) were exposed to final concentrations of SM ranging from 0.01 to 0.5 mM in culture media under sterile conditions. Biochemical and morphological parameters of SM injury were monitored at multiple time points up to 72 hours after SM addition. Untreated controls were also done under identical conditions and time points.

In the experiments in which cells were pretreated with N-acetyl-cysteine (NAC) to block apoptosis (5,17), the cells were incubated for 20 hours with 50 mM N-acetyl-L-cysteine (Sigma) (5,17). Residual NAC in the media was removed by three washings with media before SM addition.

Cell morphology. Microscopic observations of endothelial cells and keratinocytes were performed during the time course of SM injury with a Nikon optiphot microscope. Wright-Giemsa staining was performed using the Fisher LeukoStat Stain Kit.

Fluorescence microscopy. After varying periods of incubation at 37°C under the different experimental conditions, the adherent cells were fixed with 2% paraformaldehyde for 1 hr at room temperature. The paraformaldehyde was then removed and the cells were washed and permeabilized three times for 5 min with Dulbecco's Cation Free phosphate buffered saline (PBS), pH 7.4, containing 0.2% Triton X-100. Cells were stained with 165 nM rhodamine phalloidin (Molecular Probes) specific for F-actin in microfilaments (18) for 20 min at room temperature in the dark. Coverslips were sealed to each monolayer and the samples were viewed with the G filter block on a Nikon optiphot fluorescence microscope. Fluorescence micrographs were taken using TMAX 400 film (Kodak).

Assays of Cell Death. Recently many of the biochemical steps in apoptosis have been defined. Cysteine protease (caspase) activity (particularly that of caspase-3) has been identified as critical to induction of the final execution phase of apoptosis which includes destructive irreversible events involving the nucleus, plasma membrane, and cytoskeleton. It is not yet clear how caspase activity is linked to the initiation of events in the execution phase of apoptosis. Since it is possible that the actual pattern of execution phase events may depend on both stimulus and individual cell type, caspase activity may be a more reliable indicator of activation of the apoptotic death program.

Caspase-3 Measurements. Confluent or nearly confluent cultures in 6 well plates were treated with sulfur mustard (SM) at final concentrations of 0, 10, 50, 100, or 250 µM. At harvest, cells were scraped into the medium, which was transferred to microfuge tubes and centrifuged at 1500 rpm in a microfuge. Cell pellets were resuspended in 150 µL insect cell lysis buffer (PharMingen, San Diego, CA), snap frozen in liquid nitrogen and stored at -70° C. At time of assay, lysates were thawed on ice, then centrifuged 10 min at 14,000 rpm in a microcentrifuge at 4° C. Aliquots (100 µL) of the clarified lysates were used for determination of caspase-3 activity.

Caspase-3 activity was measured using a Perkin-Elmer HTS 7000 BioAssay Reader largely as described in product literature for Calbiochem's Caspase-3 colorimetric substrate I, Ac-DEVD-pNA (Calbiochem, La Jolla, CA). However, two important changes were made to the suggested protocol: 1) a fluorogenic substrate, Ac-DEVD-AMC (PharMingen, San Diego, CA) was used, with emission at 450 nm in response to excitation at 380 nm measured, and 2) protein concentrations in the lysates were determined with a Bio-Rad Assay (Bio-Rad, Hercules, CA) to allow expression of the caspase-3 activities in terms of protein. A 7-amino-4-methylcoumarin (Aldrich Chemical Co., Milwaukee, WI) 10 µM standard was included in each assay.

Determination of apoptotic (chromatin condensation-fragmentation) index and cell viability (plasma membrane integrity) (19). Cells were stained during the time course of SM injury with a dye mixture (10 µM acridine orange and 10 µM ethidium bromide; (Sigma), that was prepared in phosphate-buffered saline (PBS)).

Acridine orange (fluorescent DNA-binding) intercalates into DNA, making it appear green, and binds to RNA, staining it red-orange. Ethidium bromide is taken up only by nonviable cells, and its fluorescence overwhelms that of the acridine orange, making the chromatin of lysed cells appear orange.

At the end of each experimental time point, all of the medium was removed and cells were harvested by incubation with 0.05% trypsin and 0.02% EDTA for 1 min and washed with the medium. Then, 250 µl of cell suspension was mixed with 10 µl of the dye mix and at least 100 cells per sample were examined by fluorescence microscopy, according to the following criteria: (1) viable cells, with normal nuclei (fine reticular pattern of green stain in the nucleus and red-orange granules in the cytoplasm); (2)

apoptotic cells, with apoptotic nuclear changes (green chromatin which is highly condensed or fragmented and uniformly stained by the acridine orange); and (3) nonviable (necrotic) cells, with plasma membrane lysis (bright orange chromatin). The study of the viability of cells in the undisturbed monolayers has shown that trypsinization does not promote further cell injury.

Endonuclease activity (5). Cell samples (3 x 10^6 cells) obtained during the time course of SM injury were lysed in 750 μl of buffer (100 mM Tris, 5 mM EDTA, 200 mM NaCl, and 0.2% SDS at pH 8.5) to which Proteinase K (100 μg/ml final concentration) was added. Samples were incubated in a shaking water bath at 37° C for 1 hr. Then, DNA was precipitated by addition of an equal volume of cold isopropanol with gentle mixing. The precipitate was pelleted by centrifugation at 14,000g for 30 min, air dried (after decanting the supernatant) under a fume hood for 20 min, and then resuspended in 50 μl TE buffer (10 mM Tris, 1 mM EDTA, pH 7.6) containing 40 μg/ml RNase. Equal volumes of each sample were electrophoresed on a 1% agarose gel stained with ethidium bromide. The gel was photographed under UV light.

Detection of Apoptosis Using Annexin V. At various time points after SM treatment, the cells were harvested by trypsinization and the pattern of cell death was assessed using the flow cytometric Apoptosis Detection Kit (R&D Systems, Minneapolis, MN). The assay is based on the fact that during the apoptotic process, cells express phosphatidyl serine on the outer leaflet of the plasma membrane and will bind Annexin V. The necrotic cells are differentiated from the apoptotic cells because in the former cells the integrity of the plasma membrane has been compromised and will allow uptake of propidium iodide (PI) which binds to DNA. Viable cells are negative for both Annexin V and PI staining. The assay was performed essentially as described by the supplier. The FITC-Annexin V fluorescence was read with the FL1 photomultiplier tube (PMT) and PI fluorescence was detected using the FL3 PMT.

MTT Viability Assay. In some experiments, viability was assessed as the ability of cellular mitochondria to process 3-(4,5-dimethylthiazol-2-yl)-2,5-diphenyl-2H-tetrazolium bromide (MTT) to an insoluble blue formazan product (20). After cellular incubation for varying times following SM addition, MTT (in PBS) was added at a final concentration of 250 μg/mL. After 2 hr, the plates were centrifuged for 5 min at 1500 rpm, the medium was removed and 2 mL DMSO added. After thorough mixing, the absorbance (A) at 560 nm was measured using a Perkin-Elmer HTS-7000 BioAssay Reader. The A560 of the treatment groups was expressed as a percentage of that of the DMSO control.

ATP measurement. Cellular ATP levels were assayed as previously reported by the luciferase-luciferin method of Stanley and Williams (5). The luciferase-luciferin (Sigma) was reconstituted in a buffer containing 1% bovine serum albumin, 20 mM glycine, and 2 mM EDTA, pH 8.0. Measurements were performed in an LKB Model 1251 automated luminometer (LKB Instruments, Inc., Gaithersburg, MD). ATP data were expressed as nanomoles of ATP per 1 x 10^6 cells. The whole cell population, including any floating cells, was subjected to the assay.

Measurement of Myosin Light Chain Kinase (MLCK) activity (21).

Immunoprecipitation and blotting of phosphorylated myosin light chain. Confluent or nearly confluent cultures of human keratinocytes in 6 well plates were treated with sulfur mustard (SM) concentrations of 0, 10, 50, 100 or 250 µM for 16 hr. At harvest, the cells were scraped into the medium, which was transferred to microfuge tubes and centrifuged at 1500 rpm in a microfuge. Cell pellets were resuspended in 100 µL lysis buffer (25 mM Tris, pH 7.5; 50 mM NaF, 1.5 mM dithiothreitol, 2 mM Na_3 VO_4, 0.5% Triton X-100, 100 µM phenylmethylsulfonyl fluoride [PMSF], 10 µg aprotinin, 10 µg leupeptin), then mixed at 4° C. After 30 min, 25 µL Protein A-agarose (Sigma, St. Louis, MO) was added to each tube, which was then mixed an additional 30 min at 4° C, followed by centrifugation at 14,000 rpm for 20 min in a microfuge at 4° C. Aliquots (100 µl) of the cleared lysates were added to 0.9 mL immunoprecipitation buffer (final concentrations: 10 mM Tris, pH 7.5, 150 mM NaCL; 1% Triton X-100; 1.0% NP-40; 1 mM EDTA; 1 mM EGTA; 0.2 mM Na_3 VO_4, 0.4 mM PMSF and 0.4 mM benzamidine) and 20 µL rabbit anti-myosin IgG (Biomedical Technologies, Inc., Stoughton, MA). After mixing for 2 hr at 4° C, 50 µL Protein A-agarose was added, followed by another 2 hr mixing. IgG-Protein A-agarose complexes were recovered by 5 min centrifugation at 500 rpm in a microfuge at 4° C. After addition of 60 µL sample buffer, samples were boiled 10 min prior to being frozen and stored at -70° C. A 10 µL aliquot of each sample and a prestained standard (Bio-Rad, Hercules, CA) were electrophoresed in a 4-20% Tris-HC1 gradient gel (Bio-Rad, Hercules, CA), then transferred to a nitrocellulose membrane (Bio-Rad, Hercules, CA) with a Trans-Blot SD Transfer Cell (Bio-Rad, Hercules, CA). The membrane was blocked 2 hr in TBST (100 mM Tris, pH 7.5, 0.9% NaCl, 1% Tween-20) containing 2% BSA, then incubated overnight with rabbit anti-phosphoserine IgG (1:2000 in TBST), then for 1 hr with peroxidase-conjugated goat anti-rabbit IgG (Jackson Labs, West Grove, PA). Detection was performed with an ECL+ Kit (Amersham, Arlington Heights, IL) in conjunction with Molecular Dynamics 860-WKSN Phosphorlmager and Storm software. Annotation was added in PhotoShop 4.0.

Cytoplast preparation. Cytoplasts were prepared using a modification of the method of Roos et al. (22). Briefly, endothelial cells were incubated for 5 min. at 37° C in 12.5% Ficoll 70 with 20 μM dihydrocytochalasin B. The cells were then layered on a discontinuous gradient of 16% Ficoll 70 on 25% Ficoll 70 at 33° C. The Ficoll solutions were mixed in phosphate-buffered saline. The gradients contained dihydrocytochalasin B throughout. The gradients were spun at 81,000 G (SW-41 rotor) for 50 min. at 33° C. Cytoplasts were collected from the 12.5 to 16% interface. Control cells were incubated for 60 min. in 12.5% Ficoll 70 and dihydrocytochalasin B. The control cells and cytoplasts were washed at least four times with calcium-free MGB. The standard buffer (MGB) used for assays was the same with 1.5 mM $CaCl_2$ present. After filtration through 74 μm nylon mesh (Small Parts, Inc., Miami, FL) to remove aggregates and debris, recoveries were determined by counting leukostat stained cytospins. Volumes are estimated from forward light scatter with a Becton Dickinson (Mountain View, CA) flow cytometer (FACscan) with Becton Dickinson standard beads as references. Cytoplast viability was determined by assessing the ability of the cytoplasts to take up and concentrate calcein-AM (23). The purity of cytoplast preparations was confirmed by ethidium bromide (10 μM) staining on fluorescence microscopy demonstrating the absence of a nucleus and also by propidium iodide (PI) staining of cytoplasts on flow cytometry.

ATP depletion during SM injury. After removing the normal growth media, the adherent cells were washed twice with PBS and then incubated in the presence of glucose-free RPMI 1640 plus 5% bovine serum to which 5.5 mM glucose or no glucose and 4 mM KCN was added. After a 30 min equilibration at 37° C, the cells were treated with 0, 100, 250, or 500 μM SM. ATP levels were determined at 1, 6 and 24 hr and cellular viability was assessed at 6 and 24 hr.

Glyceraldehyde 3-phosphate dehydrogenase (GAPDH) assay (24). The activity of GAPDH in the cells was measured with a one-step assay in the forward direction as follows: Glyceraldehyde 3-phosphate + $HAsO_4^{-2}$ + $NAD^+ \xrightarrow{GAPDH}$ 3-phosphoglycerate + NADH + H^+ + $HAsO_4^{-2}$. The arsenate substitutes for phosphate and drives the reaction to the right through an unstable arsenophosphoglycerate intermediate. At 1, 3 and 6 hr after treatment with 0, 100, 250 or 500 μM SM, the cells were harvested and resuspended at 1 x 10^7 cells/ml in 30 μl sonicating buffer (0.1 M Tris-HCl and 0.5 mM EGTA) and sonicated for 30 sec. To 195 μl of sonicating buffer containing 0.2 mM NAD, 6 mM glyceraldehyde-3-phosphate, and 300 mM Na_2HAsO_4, 5 μl of sonicate was added. The initial rate of formation of NADH was monitored at 340 nm in a Perkin Elmer HTS 7000 Bio Assay Reader. For the blank, glyceraldehyde-3-phosphate was not added. The extinction coefficient for NADH is 6220 mol/$L^{-1}cm^{-1}$.

Glutathione Measurements. Total glutathione (GSH) was measured using standard methods (25,26). Briefly, 0.5 x 10^6 cells were centrifuged for 30 s in a microcentrifuge, the supernatant removed and the pellet deproteinized with 55 μl 2.5% sulfosalicylic acid in 0.2% Triton x-100. Total GSH was determined in 24-well plates using 25-μl samples for total GSH after addition of 250 μl 0.3 mM 5,5' dithiobis 2-nitrobenzoic acid (DTNB), 250 μl 0.4 mM NADPH containing 0.12 U glutathione reductase and 250 μl phosphate/imidazole buffer, pH 7.2. The difference in optical density at 412 nm was read on a Perkin-Elmer HTS 7000 BioAssay Reader.

Assay of Membrane Lipid Peroxidation (17). 1 x 10^6 cells in multiwell plates were gently washed with PBS and then to each well 1 ml PBS containing 5.5 mM glucose was added and the cells were labelled with 10 μM cis-parinaric acid (Molecular Probes) in ethanol. After 1 hr at 37° C, the cells were washed twice with fresh PBS and then treated with 0 or 500 μM alpha-tocopherol (Sigma) in ethanol for 30 min at 37° C. The cells were then injured with 0, 250 or 500 μM SM or 50 μM tert-butylhydroperoxide (positive control). After 3 hr, the cells were harvested, washed, and resuspended in PBS. The fluorescence was read using the SLM 8000C spectrofluorometer with excitation at 324 nm and emission at 413 nm.

Dihydrorhodamine 123 Assay of Intracellular Oxidant Production(27). Adherent cells were loaded with 30 μM dihydrorhodamine 123 (Molecular Probes, Eugene, OR) and then treated with 0, 250 or 500 μM SM. At 1, 2 and 3 hr post treatment, the cells were harvested by trypsinization and resuspended in MGB at 10^7 cells/ml. To 1 ml of MGB, 100 μl of cell suspension was added. Fluorescence was detected with the FL1 photomultipler tube (PMT) (488 nm excitation wavelength) on the FACScan flow cytometer (Becton-Dickinson).

Statistics. *Data have been expressed as mean ± standard deviation (S.D.) and were analyzed by two-tailed Student's t-test. Differences were considered significant where $p < 0.05$.*

RESULTS

Cell death in endothelial cells and keratinocytes induced by SM (Task 1 of SOW). We have demonstrated that endothelial cells exposed to SM concentrations ≤ 250 μM undergo the characteristic morphologic and biochemical changes typical of apoptosis including: nuclear condensation and fragmentation, endonucleolytic cleavage of DNA, cellular shrinkage, membrane budding (blebbing), actin depolymerization, and apoptotic body formation and release (5). A unique feature affecting the outer cortical band of actin filaments in endothelial cells undergoing apoptosis was the apparent constriction of this band to a much smaller ring-like structure overlying the nucleus of the shrunken apoptotic cells (5). Concentrations of SM ≥ 500 μM produced a mixed pattern of apoptosis and necrosis in the endothelial cells. The appearance of necrosis at these higher concentrations of SM correlated well with reduction of cellular ATP levels (5). In contrast, preliminary work with keratinocytes presented in the final report from our previous contract period, suggested that keratinocytes primarily undergo necrosis in response to SM. This was largely based on assays of plasma membrane integrity and nuclear morphologic features typical for apoptosis. Recent observations by Rosenthal, et. al. (13) suggest that caspase activation can occur in keratinocytes following SM exposure, thus it is possible that apoptosis and necrosis may represent a continuum with various hybrid patterns of cell death potentially occurring between the extremes, rather than two separate distinct patterns of cell death. To examine this possibility we injured the cells with 0, 10, 50, 100, and 250 μM SM over a longer time course (16, 24, 48, and 72 hours) than in our earlier work to assess keratinocytes for the presence of the classical morphological and nuclear/DNA criteria for apoptosis which we had seen in endothelial cells over a shorter time course. We also measured two additional non-nuclear parameters of apoptosis: 1) activation of caspase-3, the "central executioner" of apoptosis (4) and 2) Annexin V binding to exposed phosphatidyl serine residues translocated to the outer leaflet of the plasma membrane, an execution phase event facilitating phagocytic recognition of apoptotic cells and bodies.

Figure 1 depicts the appearance of keratinocytes 72 hours after exposure to 0-100 μM SM. Cellular shrinkage, chromatin condensation, nuclear fragmentation, and apoptotic body formation typical for apoptosis were seen (Fig. 1). Keratinocytes assayed (19) under these conditions demonstrated some evidence of the nuclear morphologic changes of apoptosis (Table 1), more than that seen earlier with higher SM concentrations, but still considerably less than that seen in SM-injured endothelial cells (5). There was still much evidence present for plasma membrane lysis (Table 1), even with low concentrations of SM (e.g. 50 μM). DNA isolated from the keratinocytes during the long time course following exposure to lower doses of SM demonstrated a variable pattern of degradation. Occasional but inconsistent DNA ladders, indicative of endonucleolytic cleavage, were seen, but smearing indicative of nonspecific DNA degradation typical for necrosis was also present (Fig. 2). Adherent keratinocytes stained with rhodamine phalloidin to visualize actin filaments demonstrated progressive loss of normal actin filament organization in dying cells over the 72-hour time course of SM injury with concentrations of SM as low as 50 μM (Fig. 3). The disruption and loss of actin filaments developed very slowly at the low concentrations of SM and was rarely present in cells exposed to 10 μM SM (Fig. 3), a concentration which was typically associated with minimal cell death over the same time course (e.g. Table 1). When Annexin V binding to phosphatidyl serine residues was measured in SM-injured keratinocytes by flow cytometry, ~16% of cells demonstrated binding 24 hours after exposure to 250 μM SM (Table 2). These increases in Annexin V binding occurred in keratinocytes with intact plasma membranes as confirmed with propidium iodide (Fig.

4), and thus were developing prior to the plasma membrane lysis seen in keratinocytes after SM exposure.

Measurement of caspase-3 activity in keratinocytes demonstrated some interesting findings (Fig. 5). Caspase-3 activity was increased in SM-injured keratinocytes, and its increased activity became evident before increased Annexin V binding was detected. There was a dose response of caspase-3 activity with progressive increases in activity particularly evident in response to 100 and 250 μM SM 16 hours after SM addition (Fig. 5). Endothelial cell caspase-3 activity was also increased over the same time course, particularly at 16 and 24 hours after SM exposure (Fig. 5).

Actin-myosin contraction induced in SM-injured cells (Task 2 - SOW).

Using an immunoprecipitation strategy in which a precipitating antibody to the heavy chain of myosin precipitates both the heavy and light chains of myosin together from cellular extracts, we have been examining the phosphorylation state of the light chain of myosin separated on polyacrylamide gels (PAGE) with antiphosphoserine immunoblotting as a measure of myosin light chain kinase (MLCK) activity. MLCK activity is required for actin-myosin contraction to occur and thus can be used as a biochemical confirmation of the apparent actin filament contraction seen in SM-injured endothelial cells stained with rhodamine phalloidin (5). In our preliminary work with this assay we have found that we can identify a band on PAGE of the appropriate molecular weight (~ 20 kd) (Fig. 6).

Inhibition of cytoskeletal function and SM-mediated cell death (Task 3 - SOW). In preliminary work with endothelial cells, we have examined the feasibility of using the specific MLCK inhibitor, ML9, to determine if we can block some or all of the changes in the actin filament system seen with SM injury. In earlier pilot studies with the HL60 human leukemic cell line we had seen evidence that ML9 pretreatment could apparently shift an apoptotic to a necrotic pattern of cell death. In our initial studies we have concentrated on determining conditions under which the cells could be treated without gross toxicity due to ML9 treatment alone. Figure 7 presents data suggesting that prolonged (17 hrs) exposure to ML9 at even 10 μM concentration is somewhat toxic to keratinocytes and endothelial cells. However, a short (1 -hour) exposure to ML9 is well tolerated (Figure 7) and may be useful if timed appropriately to match the visual and biochemical events involving actin filaments. Long-term toxicity associated with this agent will most likely preclude its being of use as a potential therapeutic agent for SM injury.

Cytoplast Studies (Task 4-SOW). We have initiated this work with preparation of enucleated endothelial cytoplasts. This has been technically more difficult than with smaller cells (e.g. HL-60 cells) for which the technique was originally described. Endothelial cytoplasts have not consistently been found at the 12.5 to 16% interface. We are currently adjusting the conditions of exposure to dihydrocytochalasin B and retrieving material found at each interface in the gradients to improve our yield and the consistency of the preparations. We anticipate that there may be additional technical difficulty with preparing keratinocyte cytoplasts because of potential differences in the response of actin filaments in epithelial cells to cytochalasins as compared to endothelial cells.

ATP-dependence of SM-induced cell death (Task 5 - SOW). Recently, it has been reported that apoptosis is a process which requires ATP (6-10). Using a combination of glucose depletion and mitochondrial inhibition with 4 mM KCN (28), we examined the hypothesis that cell death induced by SM is an ATP-dependent process. Endothelial cell ATP levels measured at 1, 6 and 24 hours after exposure to 0, 100, 250 and 500 μM SM were correlated with viability measurements at 6 and 24 hr using the assay of apoptotic nuclear features. Depletion of ATP levels (Fig. 8) to stable levels at 24 hrs which were ~50% of control was associated with modest but significant protection of endothelial cells exposed to 100 μM SM (Table 3). The effect of ATP depletion was primarily to decrease the number of cells demonstrating apoptotic nuclear features. At higher concentrations of SM (e.g. 500 μM), the effect of ATP depletion was primarily a delay in the progression into apoptosis seen at 6 hr and a later potentiating of the necrosis-inducing effects of SM at 24 hr (Table 3B). This data suggests that apoptosis induced by SM in endothelial cells requires ATP and that ATP depletion can shift SM-induced cell death to a more necrotic pattern as has been seen in other models of cell death. Work presented in the final report from the last contract demonstrated that although glutamine can partially restore ATP levels in endothelial cells injured by oxidants and thus help to shift a predominantly necrotic pattern of cell death to an apoptotic one (10), its utility in SM injury to endothelium is limited.

SM injury, ATP loss, and the activity of glyceraldehyde 3-phosphate dehydrogenase (GAPDH) in endothelial cells and keratinocytes (Task 6 - SOW). The glycolytic enzyme, GAPDH, has been demonstrated to be a target of inhibition by reactive oxygen species (ROS) (24,29). Inhibition of GAPDH by ROS partially accounts for the suppression of ATP synthesis in oxidant-injured cells (24,29). We tested the hypothesis that GAPDH might also be inhibited by SM and contribute to the ATP loss seen with higher dose SM injury in keratinocytes and endothelial cells. Figure 9 depicts the activity of GAPDH (measured spectrophotometrically) in keratinocytes and endothelial cells following exposure to 0, 250, and 500 μM SM. SM (500 μM) inhibited ~15% of the activity of GAPDH in endothelial cells as early as 3 hr after SM addition, but did not alter GAPDH activity in keratinocytes.

Reactive oxygen species (ROS) and SM injury (Task 7 - SOW). ROS have been implicated as important signalling intermediates in cell death (17). We tested the hypothesis that ROS may play a role in SM-mediated cell death. Three different assays have been used to examine the possibility that ROS may be generated during cellular injury with SM. Measurement of total and oxidized (GSSG) glutathione (GSH) has been used in models of oxidant stress as a fairly sensitive marker for the presence of ROS in tissues and cells (30). Reduction in the levels of measurable GSH (which under normal circumstances is predominantly in the reduced form) is a less specific indicator of oxidant stress than demonstration of formation of GSSG which is a highly specific marker for oxidant stress. The effect of the GSH-altering agents, buthionine sulfoximine (BSO) and N-acetyl-cysteine (NAC) (inhibitors and stimulators of GSH synthesis, respectively), on SM-mediated injury to endothelial cells was examined. Figure 10 depicts the effects of pretreatment with these GSH-altering agents on endothelial cell and keratinocytes total GSH levels1 and 6 hr after exposure to 500 μM SM. SM injury without any other treatment resulted in a significant ($p \leq 0.02$) reduction in the level of total GSH in endothelial cells (Fig. 10A). Pretreatment with 50 mM NAC resulted in a > 50% increase ($p \leq 0.02$) in the level of total GSH in uninjured endothelial cells and was also associated with preservation of GSH during SM injury (Fig. 10A). Pretreatment with 200 μM BSO caused a > 50% reduction ($p \leq 0.02$) in the level of total GSH in uninjured endothelial cells and completely blocked the enhancement of endothelial GSH levels associated with NAC pretreatment (Fig. 10A).

Consistent with the beneficial effect of NAC pretreatment on endothelial GSH levels, endothelial viability was enhanced at 6 hr after injury with 500 μM SM when GSH levels were augmented with NAC (69.3 ± 1.7% viable vs. 50.4 ± 4.0, control) (Table 4). This enhanced viability was primarily reflected in a reduction in the number of apoptotic cells (Table 4). GSH depletion with BSO treatment exacerbated SM injury (35.7 ± 8.4% viable vs. 50.4 ± 4.0%, control) and resulted in an increased number of necrotic cells (Table 4). The combination of BSO with NAC eliminated any of the beneficial effect seen with NAC alone (51.7 ± 4.7% viable vs. 50.4 ± 4.0%, control) (Table 4).

We also examined the possibility that exogenous GSH might have some protective effect on endothelial cells during SM injury. Indeed, when GSH was added an hour prior to SM exposure, there was substantial protection of the cells (Table 5). The primary effect of the GSH was to reduce the number of cells demonstrating apoptotic nuclear features. The effect of GSH appeared to be dose-related, although its benefit was limited to some extent by an associated toxicity at higher concentrations (Table 5).

The effect of the GSH-altering agents BSO and NAC on SM-mediated injury to keratinocytes was also examined. Figure 10B demonstrates the effects of pretreatment with these GSH-altering agents on total GSH levels in keratinocytes at 1 and 6 hours after exposure to 0 or 500 μM SM. Although NAC pretreatment enhanced total GSH levels early in the course of SM injury (at 1 hr), this effect was lost by 6 hr even in the control (Fig. 10B). As with endothelial cells, BSO antagonized the effect of NAC on total GSH levels in keratinocytes, but did not further potentiate the effect of SM on GSH levels. Most interestingly, real reductions in total GSH associated with SM exposure were not evident after 1 hr, but did become apparent by 6 hr (40-50% decrease) (Fig. 10B); suggesting that the metabolism of SM involving GSH is a fairly slow process. Surprisingly, pretreatment with NAC did not provide much protection for SM-injured keratinocytes (Table 6).

Since it is possible that generation of ROS within cells may be compartmentalized, we have examined other ways to assess ROS generation within cells after SM exposure. Parinaric acid, a fluorescent lipid which intercalates within the lipid bilayer of cellular membranes, loses fluorescence upon oxidation and thus can serve as an indicator of either background or supranormal levels of lipid peroxidation occurring within cellular membranes (17). Figure 11 demonstrates our initial experience with this assay during SM injury in endothelial cells. There was a background level of lipid peroxidation present in the control cells which was clearly increased in the positive control (t-butylhydroperoxide) (Fig. 11A) and which was substantially reduced when vitamin E (α-tocopherol) was present (Fig. 11B). Although a trend towards increased parinaric acid oxidation appeared to occur with SM exposure, this did not achieve statistical significance (Fig. 11A). This may partly reflect the need for more intermediate time points so that an actual rate of parinaric acid oxidation can be calculated for each condition (which we plan to do as we further examine this model).

Another approach to measuring ROS generation during SM injury we have taken is measurement of oxidation of dihydrorhodamine 123 (H_2Rh123). In cells in which ROS are being generated, H_2Rh123 is oxidized to the highly fluorescent Rh123 which is trapped in cells due to its charged state (27). This measure of cytosolic oxidative (ROS) activity thus complements the parinaric acid assay by giving specific information about cytosolic ROS generation and may also be a more sensitive indicator than GSSG levels. Figure 12 demonstrates our initial experience with this assay in SM-injured endothelial cells and keratinocytes. Again, not unlike the parinaric acid assay, our results are somewhat ambiguous and may again reflect the need for more time points so that rates of oxidation may be compared.

DISCUSSION

In our work specifically addressing Task 1 of the SOW, we have found that keratinocytes do not as readily demonstrate many of the classical features of apoptosis as do endothelial cells. This has led to initial observations suggesting that necrosis may be the predominant form of keratinocyte death induced by SM. This impression was based on measurements of plasma membrane integrity in cells injured primarily with higher concentrations of SM (>250 μM) and observed over relatively short time courses (0-6 hrs). With the recent explosion of interest in cell death, rapid additions to the basic understanding of the biochemical pathways regulating the process have occurred (4). This has necessitated the use of additional techniques to help more completely address the hypotheses to be tested in this Task. The combination of assaying for phosphatidyl serine translocation (Annexin V assay) and caspase-3 activation with a focus on longer time courses for measurement of the other cell death parameters have yielded a more complete and hopefully more accurate picture of keratinocyte death following SM exposure. The sometimes variable and ambiguous results with assays of nuclear changes associated with apoptosis probably reflect a relative lack of synchrony in the process of programmed cell death in keratinocytes compared to that seen with endothelial cells (5) and may also underscore the concept of cell death as a continuum between the classical extremes of apoptosis and necrosis. Evidence in SM-injured keratinocytes of activation of caspase-3, the "central executioner" of apoptosis, as well as a number of execution phase events (e.g. phosphatidyl serine translocation, actin filament breakdown, membrane budding, etc.) occurring over a 72-hr time course are strong indicators that programmed cell death does occur. Coupled with other evidence of DNA smearing on agarose gels and plasma membrane disruption, it appears that our earlier concept of necrosis and apoptosis induced by SM being distinct entities (5) is probably not correct. Apoptosis if allowed to proceed will occur unless metabolic or other factors supervene to produce some of the more distinctive features of necrosis. Commitment to either pattern may still entail caspase activation and thus almost all cell death will probably involve some "programmed" elements or features. Thus, we request that the use of these additional techniques, which have been so helpful, be accepted as a revision to our SOW for completion of Task 1. We plan to increase the number of replicate determinations for the viability measurements before completing Task 1.

Our concept that actin-myosin contraction may be an important element in apoptosis has been confirmed by others in a model of cell death involving PC 12 cells (21). We have made some real progress toward isolating the light chain of myosin (MLC) in Task 2 of the SOW to ultimately determine whether actin-myosin contraction, measured as MLC phosphorylation, occurs during SM injury. The technique is difficult, but we are also encouraged that we may be able to use immunoblotting with specific anti-phosphoserine antibodies and thus avoid the need for ^{32}P labeling with its associated hazards.

We have made some progress determining the condition under which we may be able to use the myosin light chain kinase inhibitor ML9 in Task 3 of the SOW. Although it may be helpful for these experiments, its toxicity will preclude its usefulness in any potential therapeutic strategy directed at treating SM-induced pathology.

In Task 5 of the SOW we have been able to reproducibly demonstrate in a model of moderate ATP depletion in endothelial cells the ATP-dependence of SM-induced apoptosis (Fig. 8, Table 3) Furthermore, these studies have also underscored the role of metabolic effects (i.e. ATP loss) in regulating the interconversion between apoptosis and necrosis and has also confirmed and extended earlier work with other models demonstrating the ATP dependence of apoptosis (6-10). This work will now need to be extended to keratinocytes to complete Task 5.

Studies of GAPDH activity in endothelial cells and keratinocytes after exposure to SM (addressing Task 6 of the SOW) demonstrate that GAPDH is minimally inhibited in endothelial cells by SM (Fig. 9). The inhibition of GAPDH at the higher concentrations of SM (>250 μM) may at least in part account for the ATP loss seen in endothelial cells after injury at these concentrations of SM. Whether GAPDH is inhibited directly by SM or indirectly by ROS generated during SM injury remains a mystery awaiting better definition of ROS activity during SM injury (in the experiments of Task 7). We plan to complete Task 6 with a larger number of replicates for the GAPDH measurements.

In our work thus far addressing Task 7 we have no clear-cut evidence yet of ROS generation during SM injury in endothelial cells and keratinocytes. Total GSH and viability measurements with and without the use of GSH-altering conditions (Fig. 10 and Table 4) confirmed and extended other observations (31-33) demonstrating loss of GSH after SM exposure as well as the GSH-dependence of protective effects associated with NAC pretreatment. As has been seen by others (34) exogenous GSH addition also provided considerable protection during SM injury (e.g. Table 5). These results are consistent with either GSH acting in SM injury as a scavenger of ROS and/or as a direct scavenger of SM itself and are thus not conclusive evidence of ROS generation during SM injury. Measurement of real increases in GSSG will be a much more specific indicator of ROS generation during SM injury and still remain to be completed.

Hockenbery, et. al. (17) have demonstrated in a physiologic (hormone-withdrawal) model of apoptosis the presence of ROS using parinaric acid oxidation within membranes and oxidation of dichlorofluorescin (a cytosolic marker of oxidation analogous to dihydrorhodamine 123) as ROS indicators. Where parinaric acid oxidation (lipid peroxidation) was inhibited either by overexpression of the proto-oncogene bcl_2 or pretreatment with NAC, apoptosis was inhibited (17). We have adopted a similar strategy to initially determine if SM-injured cells generate ROS and then to examine the role of any ROS generated in SM-induced cell death.

Our work with both the parinaric acid and dihydrorhodamine 123 assays has provided suggestive, but not yet conclusive evidence for ROS generation during SM injury. As was suggested in the Results section, these assays will be more reliable when more time points are monitored so that rates of oxidation can be determined (especially since it appears that there may be background oxidation occurring). With further refinement of these assays and the concurrent use of antioxidants during SM injury, we hope to obtain more definitive information regarding ROS generation during SM injury and their role in SM-mediated cell death. If with these refinements we obtain clearly negative results, further measurements directed at assaying for DNA base oxidation will be of little value.

CONCLUSIONS

The work presented in this mid-term report has helped to clarify the nature of cell death induced in endothelial cells and keratinocytes by SM. Although the "classic" features of apoptosis are demonstrated in a fairly rapid and synchronous manner in endothelial cells (5), keratinocyte death after SM exposure does not always demonstrate consistently all the features of apoptosis. Features of necrosis are often mixed with markers for apoptosis in keratinocytes and may simply reflect a less synchronous execution of the death program in keratinocytes compared to endothelial cells. These results are important confirmation of other work (13), and suggest that therapeutic strategies directed at central elements of the cell death program (e.g. caspases) may be extremely relevant to the development of effective countermeasures to SM. These studies are also consistent with the concept that cell death may represent a continuum - the extremes of which are classical apoptosis and necrosis. Finally, the slower, less synchronous pattern of keratinocyte loss after SM injury in comparison to the pattern of SM-induced endothelial cell death is consistent with the probable sequence of pathogenic events underlying SM-induced vesication (i.e. capillary leak develops first, with the relatively rapid loss of endothelial monolayer function, followed secondarily by edema fluid accumulation under the basal keratinocyte layer which loses adherence as an early element in its slower process of programmed death, thereby resulting in micro- and eventual macro-blister formation).

REFERENCES

1. Schwartzman, R.A. and Cidlowski, J.A. Apoptosis: the biochemistry and molecular biology of programmed cell death. Endocrine Rev. 14:133-151, 1993.
2. Schwartz, L.M. and Osborne, B.A. Programmed cell death, apoptosis and killer genes. Immunol. Today 14:582-590, 1993.
3. Gerschenson, L.E. and Rotello, R.J. Apoptosis: a different type of cell death. FASEB J. 6:2450-2455, 1992.
4. Hetts, S.W. To die or not to die: An overview of apoptosis and its role in disease. JAMA 279:300-307, 1998.
5. Dabrowska, M.I., Becks, L.L., Lelli, Jr., J.L., Levee, M.G., and Hinshaw, D.B. Sulfur mustard induces apoptosis and necrosis in endothelial cells. Toxicol. Appl. Pharmacol. 141:568-583, 1996.
6. Leist, M., Single, B., Castoldi, A.F., Kuhnle, S., Nicotera, P. Intracellular adenosine triphosphate (ATP) concentration: A switch in the decision between apoptosis and necrosis. J. Exp. Med. 185:1481-1486, 1997.
7. Eguchi, Y., Shimizu, S., and Tsujmoto, Y. Intracellular ATP levels determine cell death fate by apoptosis or necrosis. Cancer Res. 57:1835-1840, 1997.
8. Stefanelli, C., Bonavita, F., Stanie, I., Farruggia, G., Falcieri, E., Robuffo, I., Pignatti, C., Muscari, C., Rossoni, C., Guarnieri, C., Caldarerra, C.M. ATP depletion inhibits glucocorticoid-induced thymocyte Apoptosis. Biochem. J. 322:909-917, 1997.

9. Kass, G.E.N., Eriksson, J.E., Weis, M., Orrenius, S., and Chow, S.C. Chromatin condensation during apoptosis requires ATP. Biochem. J. 318:749-752, 1996.

10. Lelli, Jr., J.L., Becks, L.L., Dabrowska, M.I., and Hinshaw, D.B. ATP converts necrosis to apoptosis in oxidant-injured endothelial cells. Free Rad. Biol. Med. in press, 1998.

11. Nagata, S. Apoptosis by death factor. Cell 88:355-365, 1997.

12. Alnemri, E.S., Livingston, D.J., Nicholson, D.W., Salvesen, G., Thornberry, N.A., Wong, W.W., and Yuan, J. Human ICE/CED-3 protease nomenclature. Cell 87(2):171, 1996.

13. Rosenthal, D.S., Rosenthal, C.M.G., Iyer, S., Smith, W., Ray, R., and Smulson, M.E. Calmodulin and caspases mediate SM-induced terminal differentiation and apoptosis in keratinocytes. Proceedings of USAMRMC 1998 Bioscience Review. in press. (presented 3 June 1998, Hunt Valley, MD).

14. Mitra, R.S., Wrone-Smith, T., Simonian, P., Foreman, K.E., Nunez, G., and Nickoloff, B.J. Apoptosis in keratinocytes is not dependent on induction of differentiation. Lab. Invest. 76:99-107, 1997.

15. Korb, L.C. and Ahearn, J.M. Clq binds directly and specifically to surface blebs of apoptotic human keratinocytes: Complement deficiency and systemic lupus erythematosus revisited. J. Immunol. 158:4525-4528, 1997.

16. Leverkus, M., Yaar, M., and Gilchrest, B.A. Fas/Fas ligand interaction contributes to UV-induced apoptosis in human keratinocytes. Exp. Cell Res. 232:255-262, 1997.

17. Hockenbery, D.M., Altvai, Z.N., Yin, X-M, Milliman, C.L., and Korsmeyer, S.J. Bcl-2 functions in an antioxidant pathway to prevent apoptosis. Cell 75:241-251, 1993.

18. Wulf, E., Deboren, A., Bantz, F.A., Faulstich, H., and Wieland, T.H. Fluorescent phallotoxin, a tool for the visualization of cellular actin. Proc. Natl. Acad. Sci. USA 76:4498-4502, 1979.

19. Duke, R.C. and Cohen, J.J. Morphological and biochemical assays of apoptosis. Current Protocols in Immunology Suppl. 3.17:1-16, 1992.

20. Mosmann, T. Rapid colorimetric assay for cellular growth and survival: Application to proliferation and cytotoxicity assays. J. Immunol. Meth. 65:55-63, 1983.

21. Mills, J.C., Stone, N.L., Erhardt, J., and Pittman, R.N. Apoptotic membrane blebbing is regulated by myosin light chain phosphorylation. J. Cell Biol. 140:627-636, 1998.

22. Roos, D., Voetman, A.A., and Meerhof, L. J. Functional activity of enucleated human polymorphonuclear leukocytes. J. Cell Biol. 97:368-377, 1983.

23. Hinshaw, D.B., Miller, M.T., Omann, G.M., Beals, T.F., and Hyslop, P.A. A cellular model of oxidant-mediated neuronal injury. Brain Res. 615:13-26, 1993.

24. Hinshaw, D.B., Burger, J.M., Delius, R.E., and Hyslop, P.A. Mechanism of protection of oxidant-injured endothelial cells by glutamine. Surgery 108:298-304, 1990.

25. Brehe, J.E., and Burch, H.B. Enzymatic assay for glutathione. Anal. Biochem. 74:189, 1976.

26. Griffith, O.W. Determination of glutathione and glutathione disulfide using glutathione reductase and 2-vinyl-pyridine. Anal. Biochem.106:207, 1980.

27. Royall, J.A. and Ischiropoulos, H. Evaluation of 2",7'-Dichlorofluorescin and Dihydrorhodamine 123 as Fluorescent Probes for Intracellular H_2O_2 in Cultured Endothelial Cells. Arch. Biochem. Biophys. 302:348-355, 1993.

28. Hinshaw, D.B., Burger, J.M., Miller, M.T., Adams, J.A., Beals, T.F., and Omann, G.M. ATP depletion induces an increase in the assembly of a labile pool of polymerized actin in endothelial cells. Am. J. Physiol. 264 (Cell Physiol. 33):C1171-C1179, 1993.

29. Hyslop, P.A., Hinshaw, D.B., Halsey, W.A., Jr., Schraufstatter, I.U., Sauerheber, R.D., Spragg, R.G., Jackson, J.H., Cochrane, C.B. Mechanisms of oxidant-mediated cell injury: The glycolytic and mitochondrial pathways of ADP phosphorylation are major intracellular targets inactivated by hydrogen peroxide. J. Biol. Chem. 263:1665, 1988.

30. Schraufstatter, I.U., Hinshaw, D.B., Hyslop, P.A., Spragg, R.G., and Cochrane, C.G. Glutathione cycle activity and pyridine nucleotide levels in oxidant-induced injury of cells. J. Clin. Invset. 76:1131-1139, 1985.

31. Langford, A.M., Hobbs, M.J., Upshall, D.G., Blain, P.G., Williams, F.M. The effect of sulphur mustard on glutathione levels in rat lung slices and the influence of treatment with arylthiols and cysteine esters. Human & Exp. Toxicol. 15(8):619-624, 1996.

32. Ray, R., Legere, R.H., Majerus, B.J., Petrali, J.P. Sulfur mustard-induced increase in intracellular free calcium level and arachidonic acid release from cell membrane. Toxicol. & Applied Pharm. 131(1):44-52, 1995.

33. Gross, C.L., Innace, J.K., Hovatter, R.C., Meier, H.L., and Smith, W.J. Biochemical manipulation of intracellular glutathione levels influences cytotoxicity to isolated human lymphocytes by sulfur mustard. Cell Biol. & Toxicol. 9:259-267, 1993.

34. Smith, C.N., Lindsay, C.D., Upshall, D.G. Presence of methenamine/glutathione mixtures reduces the cytotoxic effect of sulphur mustard on cultured SVK-14 human keratinocytes in vitro. Human & Exp. Toxicol. 16(5):247-253, 1997.

FIGURE LEGENDS

Figure 1. Micrographs of SM-treated keratinocytes. Keratinocytes grown in six-well plates were treated with 0, 10, 50, and 100 μM SM and stained with Wright-Giemsa after 72 hours. A) 0 μM SM; B) 10 μM SM; C) 50 μM SM; D) 100 μM SM. Note the appearance of apoptotic bodies at 50 μM (C) and 100 mM (D) SM. 400X original magnification.

Figure 2. Degradation of keratinocyte DNA after SM injury. Cells grown in six-well plates were treated with 0, 50, 100 or 250 μM sulfur mustard for 16, 24, 48 or 72 hr. The cells were harvested and cellular DNA prepared as described in the Methods. The lanes are as follows: A) lanes 1-5 (16 hr) and 6-10 (24 hr) are 0, 10, 50, 100 and 250 μM SM, respectively. B) lanes 1-5 (48 hr) are 0, 10, 50, 100 and 250 μM SM and lanes 6-9 (72 hr) are 0, 10, 50 and 100 μM SM, respectively (250 μM SM for 72 hr was not performed due to the large percentage of necrotic cells at 48 hr). Note the variable pattern of degradation (DNA ladders and DNA smearing) on the gel, including 0 μM SM, and compare to the percentage viable in Table 1.

Figure 3. Fluorescence micrographs of microfiliments in SM-injured keratinocytes. Keratinocytes grown in six-well plates were treated with 0, 10 or 50 μM SM and were stained with rhodamine phalloidin at the times indicated. A) 0 μM SM, 72h; B) 50 μM SM, 24h; C) 50 μM SM, 48h; D) 50 μM SM, 72h; E) 10 μM SM, 72h. Note the progressive disruption of cytoskeletal organization with 50 μM SM (B-D) and the appearance of many apoptotic cells at 72 hr. 400X original magnification.

Figure 4. The effect of SM on keratinocyte viability was assessed flow cytometrically using annexin V binding (a measure of apoptosis) and propidium iodide (PI) staining (an indicator of necrosis) as described in the methods. Dot plots (A-E) are for cells at 24 hr after treatment with 0, 10, 50, 100 and 250 μM SM, respectively. Cells in the lower left quadrants are viable cells (annexin and PI negative). Cells in the lower right quadrants are apoptotic (annexin positive). Cells in the upper quadrants are necrotic cells (PI positive). The dot plots are from a representative experiment repeated three times. Note the increase in the

number of apoptotic cells in the lower right quadrants of panels C and D. In panel E, note the shift in the population to the upper quadrants, an indication of a loss of membrane integrity.

Figure 5. Caspase-3 activities in sulfur mustard-treated human keratinocytes (Panel A) and bovine endothelial cells (Panel B). Cultures were treated with 0, 10, 50 or 100 μM sulfur mustard and harvested at indicated intervals after treatment. Caspase-3 activities were determined as described in Experimental Methods and Procedures. Graphs indicate mean ± SD for indicated number of replicates.

Figure 6. Western blot analysis of myosin light chain phosphorylation in response to sulfur mustard treatment. Human keratinocytes were harvested 16 hr after treatment with 0, 10, 50, 100, or 250 μM sulfur mustard. Myosin complexes were immunoprecipitated with a myosin heavy chain-specific antibody, electrophoresed and transferred to a membrane as described in Experimental Methods and Procedures. Probing with an anti-phosphoserine antibody detected a band of ~20 kDa, putatively the myosin light chain (indicated by arrow).

Figure 7. Viability of human keratinocytes and bovine endothelial cells in response to 1 or 17 hr (overnight) treatment with ML-9 or sulfur mustard, or both. Cultures were treated with 10 or 40 μM ML-9, 100 μM sulfur mustard, or a combination and harvested 17 hr later. For 1-hr exposures (Panels C, D), the medium was changed 1 hr post-treatment. Viability (MTT assay) was measured as described in Experimental Methods and Procedures and is expressed as a percent of the control for each replicate. Graphs indicate mean ± SD for the indicated number of replicates.

Figure 8. The effect of SM on ATP levels in endothelial cells. Cells incubated in the absence (A) or presence (B) of ATP depletion conditions described in the Methods were treated with 0-500 μM SM and harvested at 1, 6 and 24 hr. The ATP levels were determined as previously described.

Figure 9. The effect of SM on glyceraldehyde-3-phosphate dehydrogenase (GAPDH) activity was determined in endothelial cells (A) and keratinocytes (B) as described in the methods. The activity is expressed as the rate of NAD reduction measured at 340 nm. n=3

Figure 10. Effects of buthionine sulfoximine (BSO) and N-acetyl-cysteine (NAC) on GSH levels in SM-treated endothelial cells (A) and keratinocytes (B). After an overnight treatment with BSO and NAC, controls and cells treated with 500 μM SM were harvested at 1 and 6 hrs post injury and the total GSH levels were determined as described in the methods. n=3-6

Figure 11. Effect of SM on lipid peroxidation in endothelial cells. Parinaric acid labeled cells were treated with SM or tert-butylhydroperoxide (t-BuOOH) in the absence (A) or presence (B) of 500 μM alpha-tocopherol. Fluorescence was read at 1 and 3 hr using a spectroflurometer. Data are expressed as a percent of the control at 1 hr (minus alpha-tocopherol). n=3

Figure 12. Measurement of oxidant production in SM-treated endothelial cells and keratinocytes using dihydrorhodamine-123 (H2Rhd-123). Control and SM-treated cells labeled with 30 μM h2Rhd-123 were harvested at 3 hr and the fluorescence was read using a FACScan flow cytometer. n=3-4.

TABLE 1 Effect of Sulfur Mustard on Keratinocyte viability.

16 hr

μM SM	%Viable	%Apoptotic	%Necrotic
0	91.4± 3.7	0.4± 0.5	8.6± 3.8
10	85.1±10.5	3.3± 3.7	13.1± 8.3
50	68.4±17.0	10.6±11.1	14.6± 9.7
100	71.2±15.7	12.1± 8.2	16.8±14.0
250	58.1±14.8	16.4±10.8	25.6±11.3

24 hr

μM SM	%Viable	%Apoptotic	%Necrotic
0	86.8± 5.0	2.3± 1.7	10.9± 5.0
10	71.4± 8.9	14.0±11.2	14.7± 6.3
50	70.9±12.2	18.1±15.4	13.9± 5.1
100	63.7± 7.1	12.8± 4.8	23.5±10.2
250	41.1±15.6	19.9± 5.0	39.0±12.1

48 hr

μM SM	%Viable	%Apoptotic	%Necrotic
0	83.4± 7.9	3.7± 3.7	14.6± 7.3
10	71.5±15.1	2.7± 2.1	25.8±13.8
50	60.7±21.7	2.4± 2.5	36.7±22.8
100	41.8±13.5	5.6± 3.2	52.5±16.1
250	12.0± 4.2	5.6± 2.9	82.4± 6.1

72 hr

μM SM	%Viable	%Apoptotic	%Necrotic
0	78.1±13.4	3.3± 2.9	18.5±15.4
10	64.3±26.9	5.7± 8.7	29.9±27.6
50	60.3±27.8	3.3± 3.2	36.6±28.8
100	35.3±24.1	5.3± 4.6	61.0±26.2

Cells grown in six-well plates were treated with sulfur mustard at the concentrations and for the times indicated. Cells were trypsinized and stained with a mixture of acridine orange and ethidium bromide as described in the Methods. At least 100 cells were counted and the number for each category (i.e. Viable (V), Apoptotic (A) or Necrotic (N)) represents the mean percentage of total cells counted demonstrating that pattern. (n=5).

TABLE 2 Viability Determination in SM-Treated Keratinocytes using Annexin V and Propidium Iodide.

24 hr

µM SM	%Viable	%Apoptotic	%Necrotic
0	85.9±9.2	3.6±1.4	7.9±5.5
10	81.1±5.8	6.2±5.9	6.8±3.4
50	69.7±8.6	11.4±8.8	11.7±7.2
100	69.1±9.8	13.9±3.6	12.3±4.4
250	52.1±23.4	16.7±5.8	22.8±6.2

48 hr

µM SM	%Viable	%Apoptotic	%Necrotic
0	84.1±3.7	4.6±1.9	11.2±3.8
10	71.0±6.6	7.5±4.2	21.5±5.2
50	64.9±10.3	8.6±1.5	26.5±11.8
100	46.2±10.7	18.0±8.3	35.8±5.9
250	14.9±9.3	29.9±17.2	54.9±8.2

72 hr

µM SM	%Viable	%Apoptotic	%Necrotic
0	80.6±10.4	4.2±3.0	14.4±8.5
10	73.9±13.9	5.8±4.9	17.4±11.6
50	67.2±11.1	7.4±2.4	22.7±12.8
100	32.4±18.6	26.8±18.1	38.7±6.1

Control and SM-Treated keratinocytes were harvested at 24, 48 and 72 hr and stained with FITC-conjugated annexin V and propidium iodide. The fluorescence was read on a FACScan flow cytometer. N=3.

Table 3A. Effect of ATP Depletion on Sulfur Mustard Injury in Endothelial Cells (6H)

		µM SM			
	ATP Depletion	0	100	250	500
%V	Y	91.5±5.06	86.5±4.44	83.25±3.59	67.5±10.02
%V	N	91.5±2.38	86.75±4.5	82.25±2.75	53.25±15.04
%A	Y	1.5±0.58	2.5±1.0	5.75±.96	13.25±6.45
%A	N	1.75±0.5	5.0±2.94	8.5±2.89	27.0±8.29
%N	Y	7.0±4.97	11.0±3.65	11.0±2.83	19.5±5.75
%N	N	6.75±2.22	8.25±3.30	9.25±1.71	19.8±8.5

Table 3B. Effect of ATP Depletion on Sulfur Mustard Injury in Endothelial Cells (24H)

		µM SM			
	ATP Depletion	0	100	250	500
%V	Y	89.66±2.52	66.33±10.41	19.0±10.15	4.0±1.41
%V	N	88.67±2.89	56.33±7.64	17.67±10.02	11.5±12.02
%A	Y	1.67±1.15	20.33±11.24	52.0±11.14	12.5±7.78
%A	N	3.0±0.0	38.0±12.49	60.67±22.5	31.5±17.68
%N	Y	8.67±2.89	12.33±1.53	27.67±8.14	83.5±6.36
%N	N	6.67±2.89	10.33±2.52	20.67±14.15	57.0±29.70

Endothelial cells were incubated in the presence or absence of ATP depletion conditions as described in the Methods and then injured with 0-500 µM SM. Cellular viability was determined at 6 hr (A) and 24 hr (B) using the acridine orange and ethidium bromide staining method described in the text.

Table 4. Effects of BSO and NAC on sulfur mustard-treated endothelial cells.

	Control			500 µM SM		
	%V	%A	%N	%V	%A	%N
Untreated	90.3±3.1	3.6±2.1	6.1±2.8	50.4±4.0	33.1± 5.0	16.3± 4.5
0.2 mM BSO	91.0±3.0	2.7±0.6	6.3±3.1	35.7±8.4	32.7±10.3	31.7±17.8
50 mM NAC	93.3±3.6	2.5±1.0	4.3±2.6	69.3±1.7	21.2± 4.3	9.5± 4.4
BSO + NAC	92.7±4.0	2.0±1.0	5.3±3.2	51.7±4.7	37.0± 5.7	11.3± 1.2

Endothelial cells were pretreated overnight with 0.2 mM and 50 mM NAC as described in the Methods and then treated with 0 or 500 µM SM. Six hours later, the viability was determined using the acridine orange and ethidium bromide assay described in the Methods.

Table 5. Effect of exogenous GSH on sulfur mustard-induced injury in endothelial cells.

	Control			500 μM SM		
	%V	%A	%N	%V	%A	%N
mM GSH						
0	90.3±3.1	3.6±2.1	6.1±2.8	50.4±4.0	33.1±5.0	16.3±4.5
2.5	88.0±0.0	5.0±2.6	7.0±2.6	72.7±5.9	15.7±5.5	1.7±4.2
5.0	88.0±5.5	4.8±2.5	9.8±5.6	75.4±5.6	11.3±1.3	11.3±4.2
10	83.0±4.0	4.0±1.7	13.3±3.0	66.7±6.4	10.7±3.2	23.0±3.6

Cells treated with 0-10 mM GSH were treated with 0 or 500 μM SM. After six hours, the viability was determined using the acridine orange and ethidium bromide assay decribed in the Methods.

TABLE 6 Effects of Buthionine Sulfoximine(BSO) and N-acetyl-cysteine (NAC) on SM injury in Keratinocytes.

0.2 mM BSO	50 mM NAC	500µM SM	%Viable	%Apoptotic	%Necrotic
-	-	-	84.6±0.73	5.8±0.74	9.6±0.93
-	-	+	80.9±2.01	6.9±0.35	12.2±1.77
+	-	-	86.0±2.26	4.8±1.48	9.2±1.28
+	-	+	70.0±1.71	6.7±2.40	23.3±2.10
-	+	-	87.4±2.44	4.1±2.69	8.5±0.92
-	+	+	79.0±3.22	7.2±1.10	13.8±2.40
+	+	-	89.9±2.23	4.5±1.43	5.6±0.43
+	+	+	80.7±3.84	6.4±2.03	12.9±3.00

Keratinocytes were pretreated overnight with 0.2 mM BSO and 50 mM NAC as described in the methods and then injured with 0 or 500 µM SM. Six hours later, the viability was determined using the annexin V/propidium iodide assay. N=3

Figure 1a

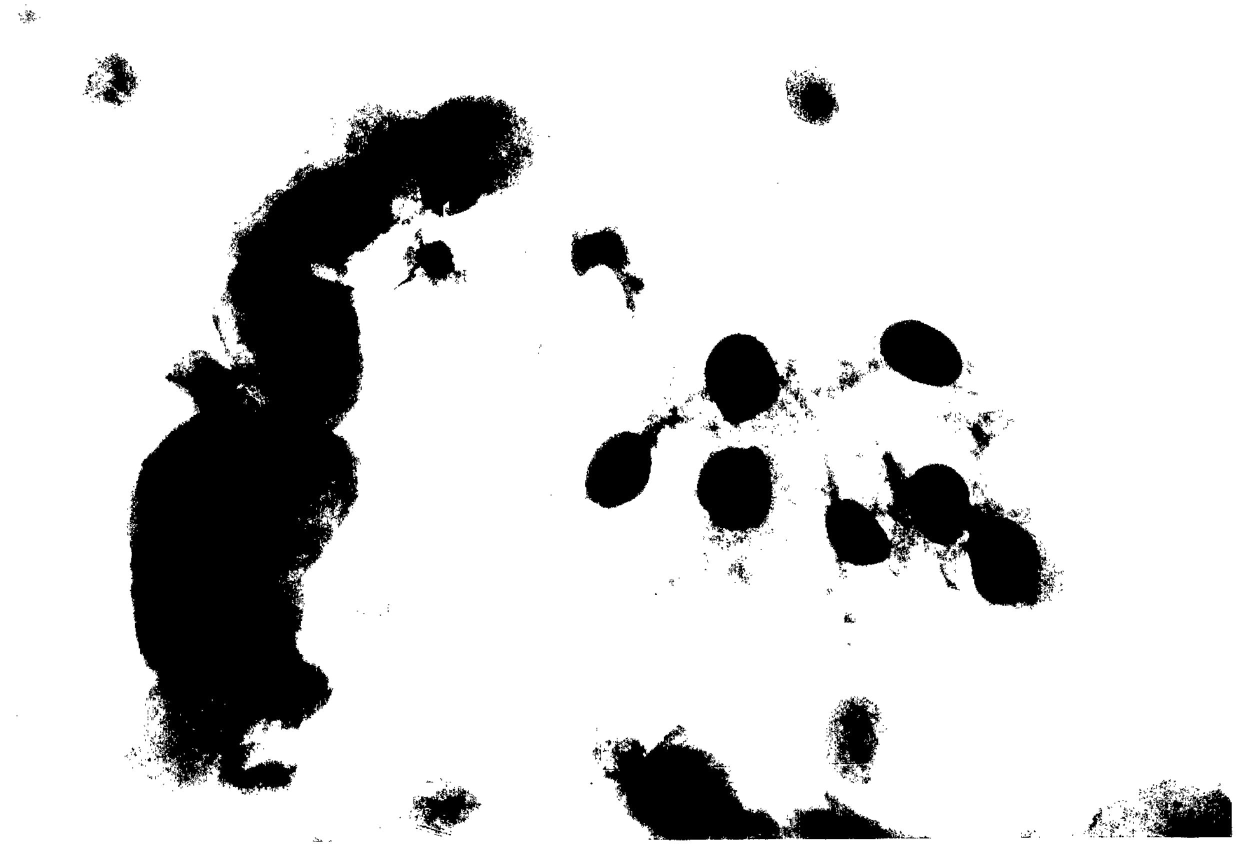

Figure 1b

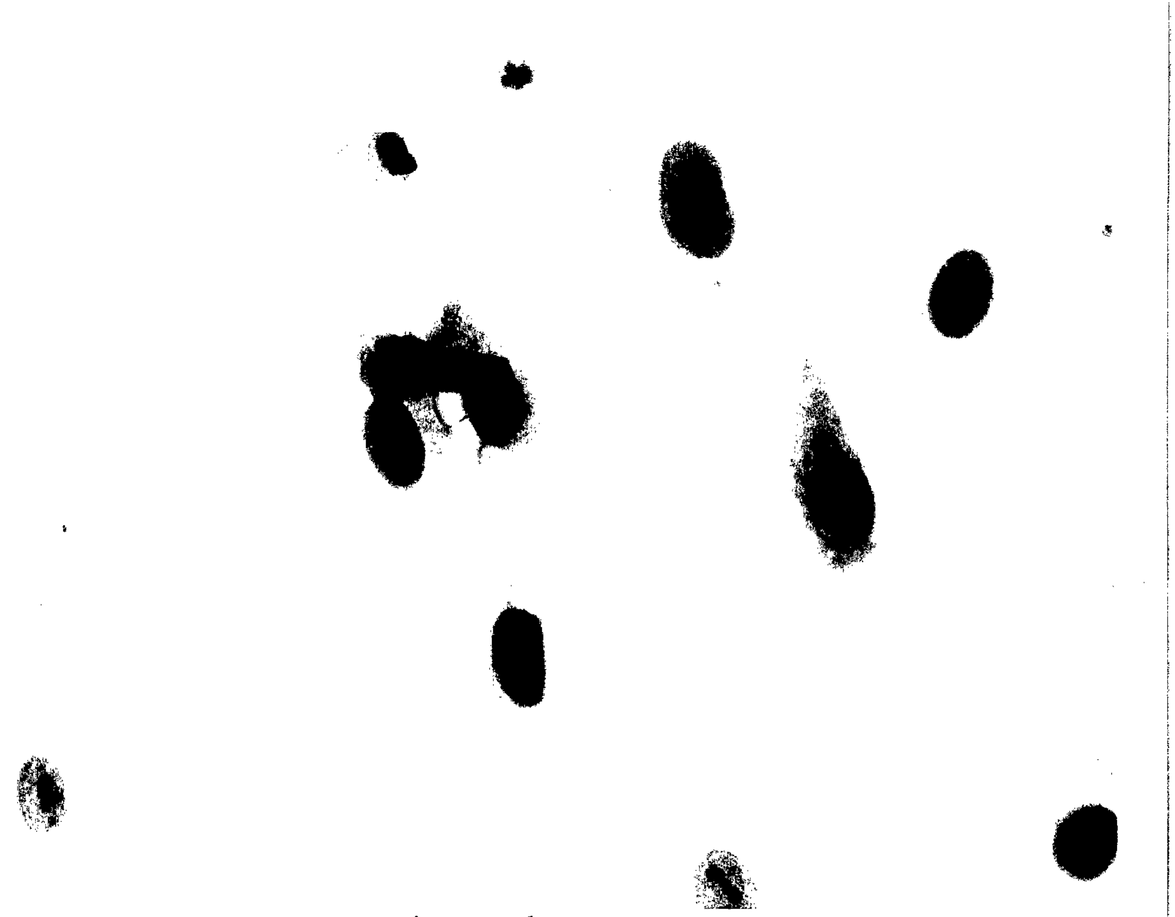

Figure 1c

Figure 1d

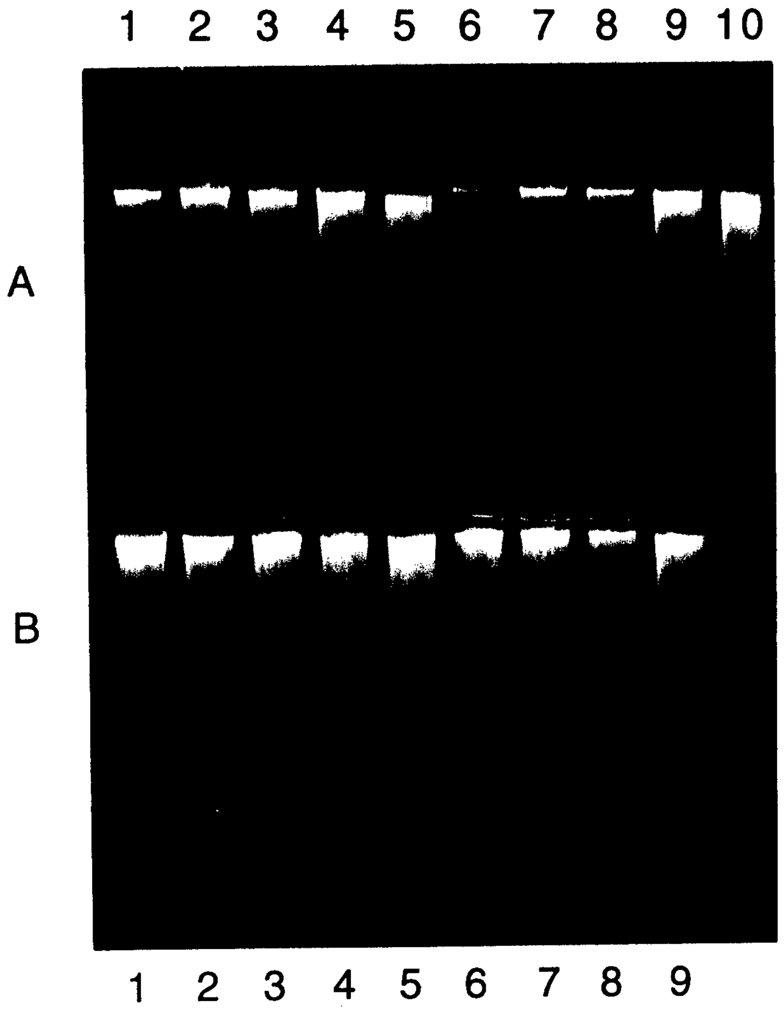
1 2 3 4 5 6 7 8 9 10
A
B
1 2 3 4 5 6 7 8 9

Figure 2

Figure 3a

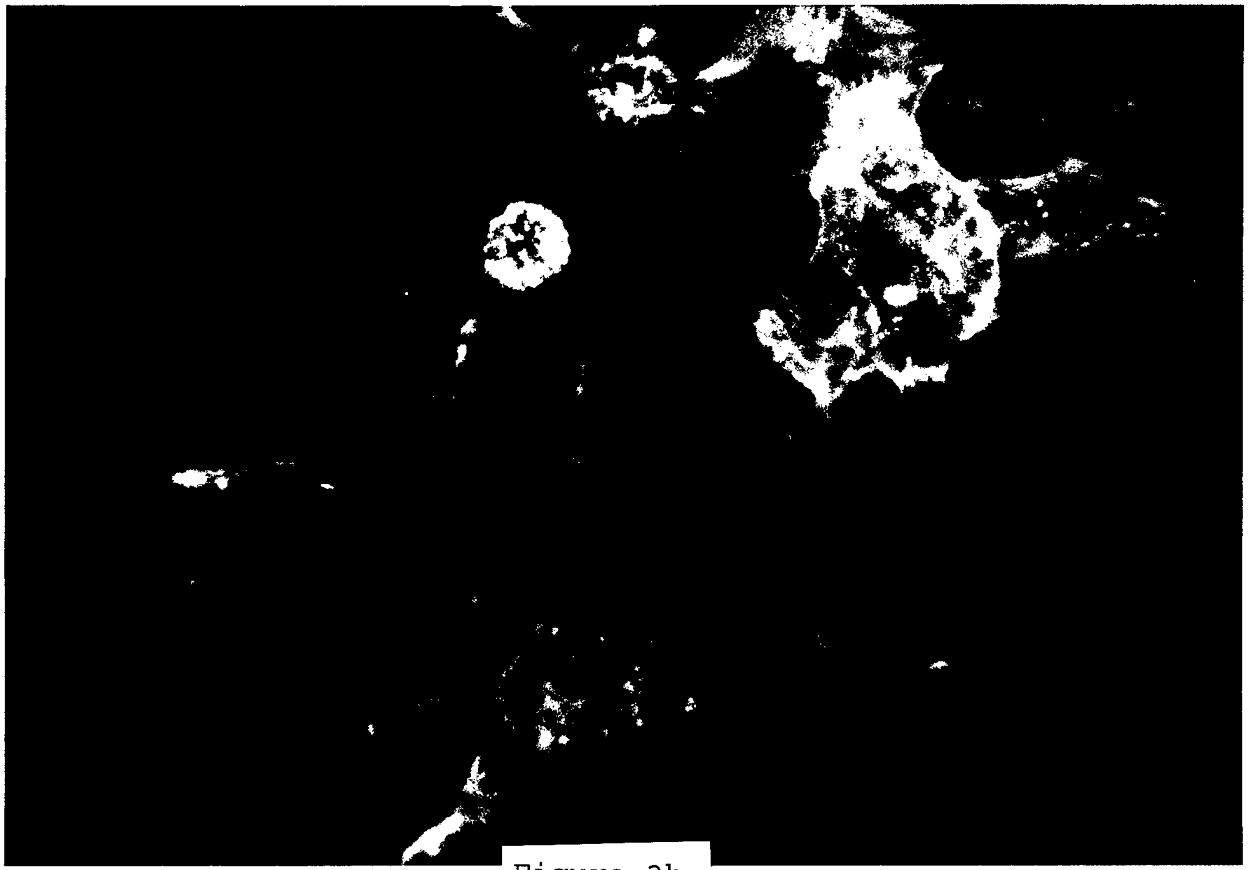

Figure 3b

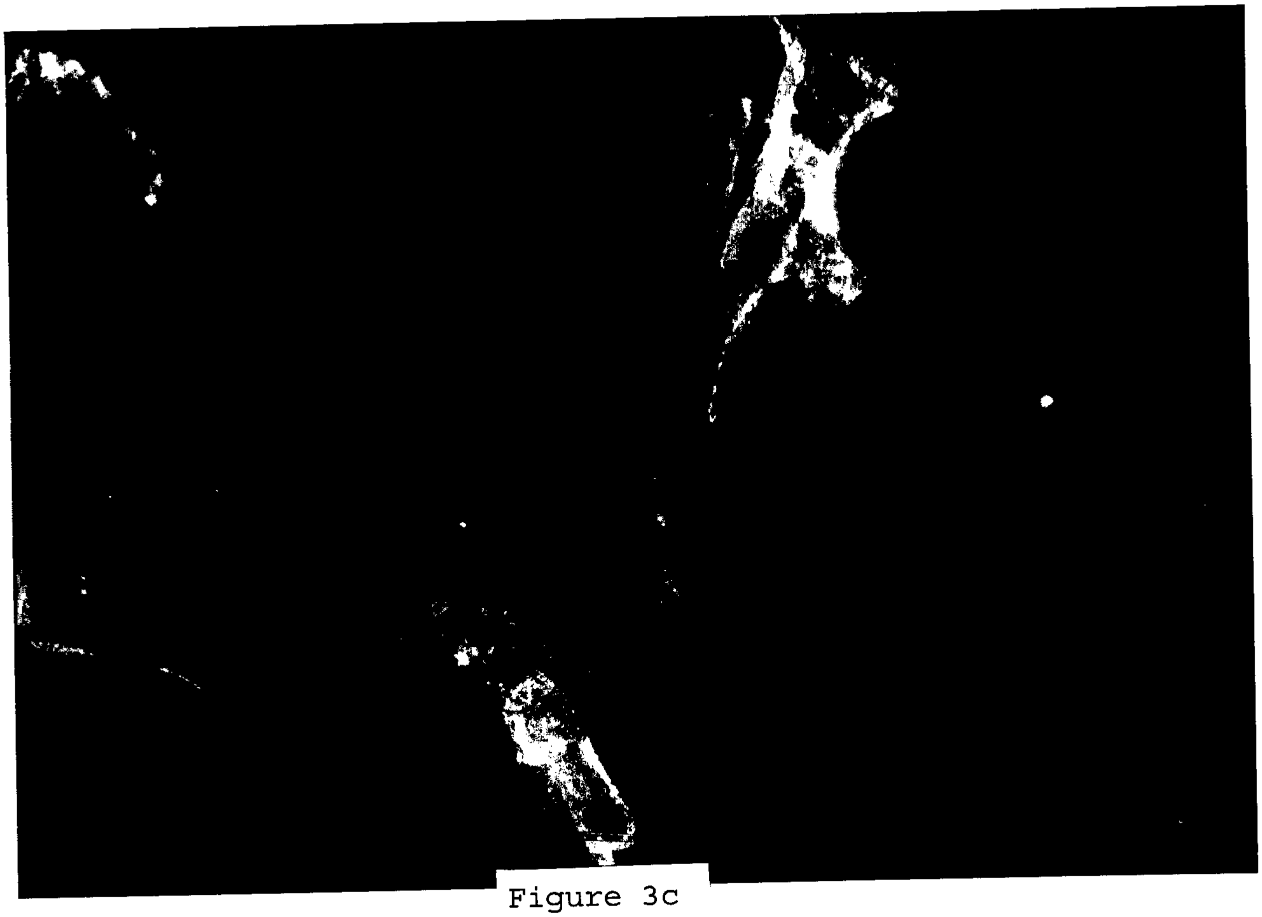

Figure 3c

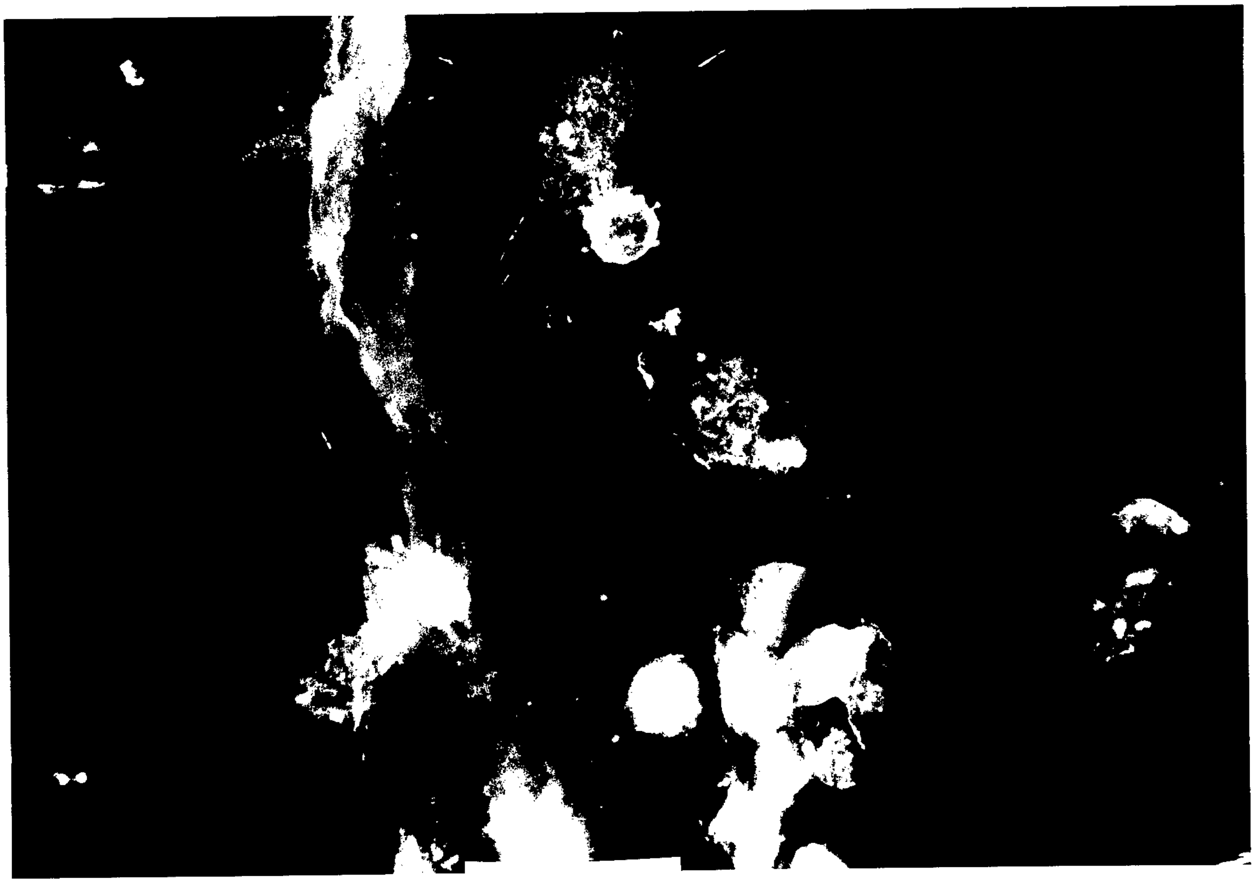

Figure 3d

Figure 3e

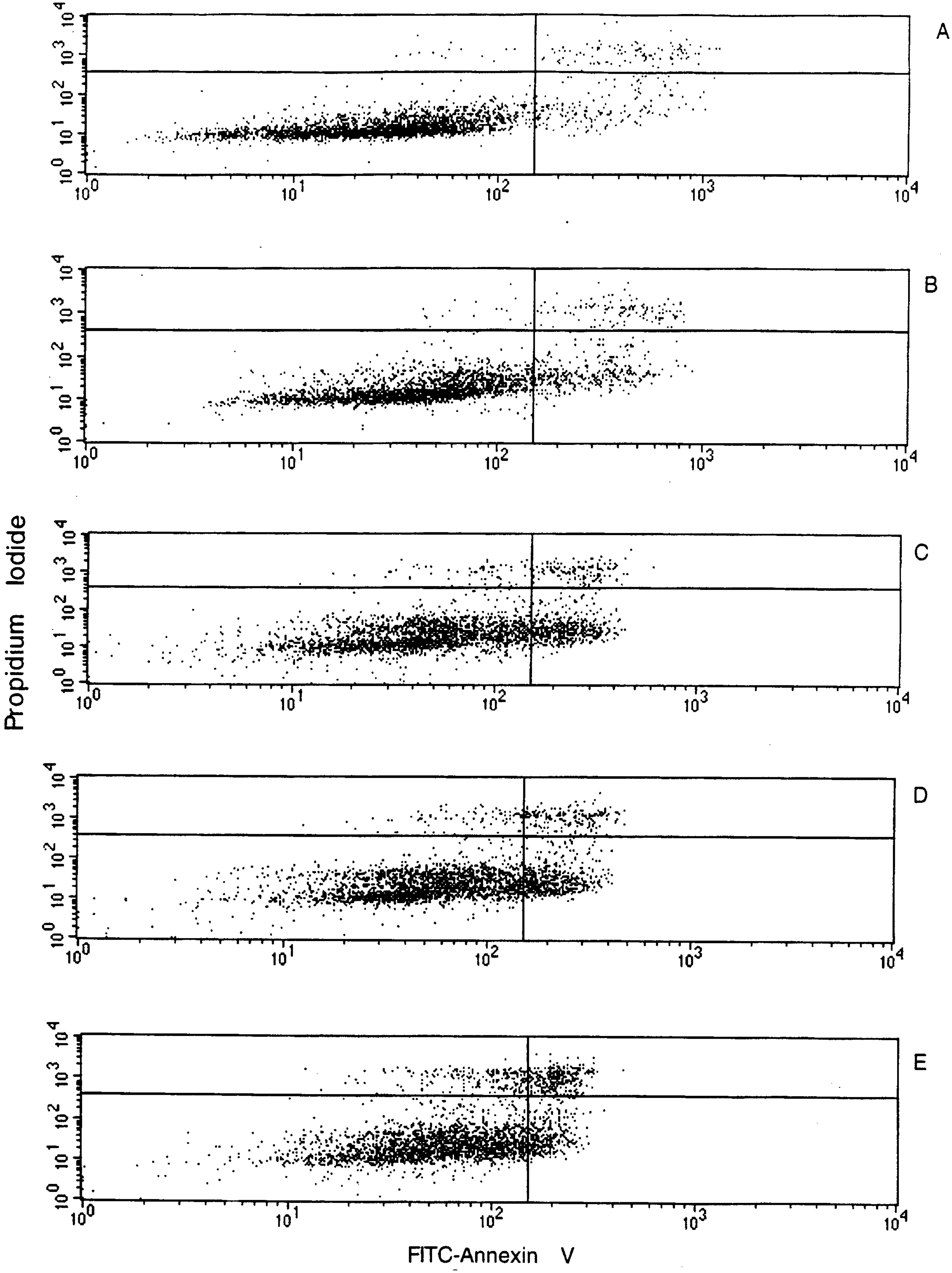

Fig. 4

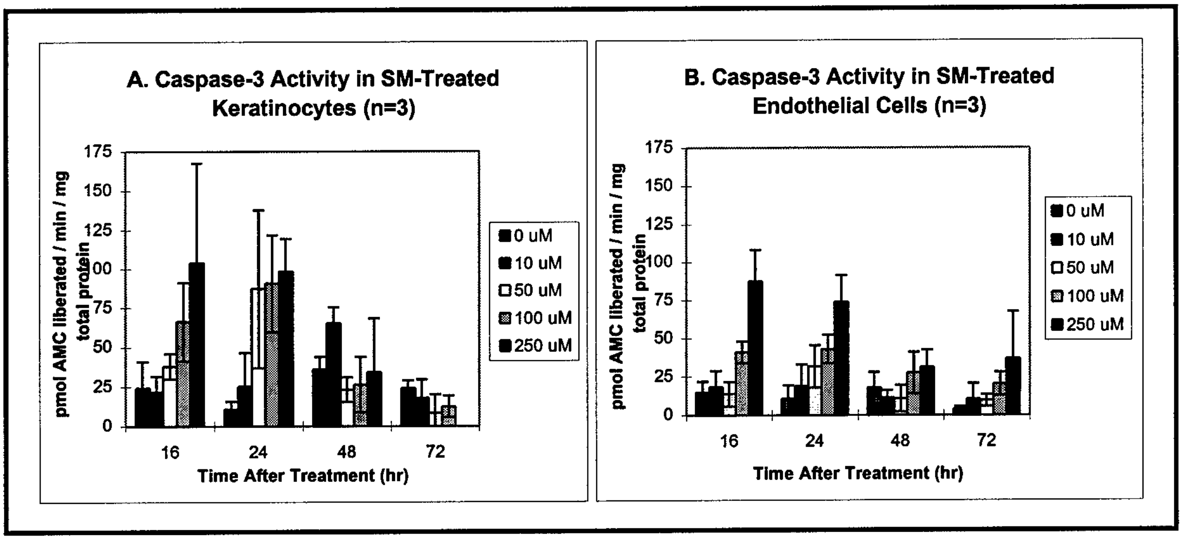
A. Caspase-3 Activity in SM-Treated Keratinocytes (n=3)
pmol AMC liberated / min / mg total protein
175
150
125
100
75
50
25
0
16
24
48
72
Time After Treatment (hr)
■ 0 uM
■ 10 uM
□ 50 uM
▨ 100 uM
■ 250 uM
B. Caspase-3 Activity in SM-Treated Endothelial Cells (n=3)
pmol AMC liberated / min / mg total protein
175
150
125
100
75
50
25
0
16
24
48
72
Time After Treatment (hr)
■ 0 uM
■ 10 uM
□ 50 uM
▨ 100 uM
■ 250 uM

Fig. 5

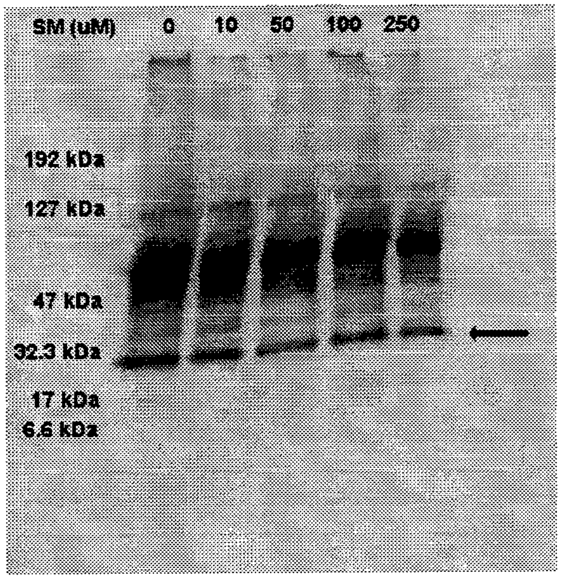
SM (uM)
0
10
50
100
250
192 kDa
127 kDa
47 kDa
32.3 kDa
17 kDa
6.6 kDa

Fig. 6

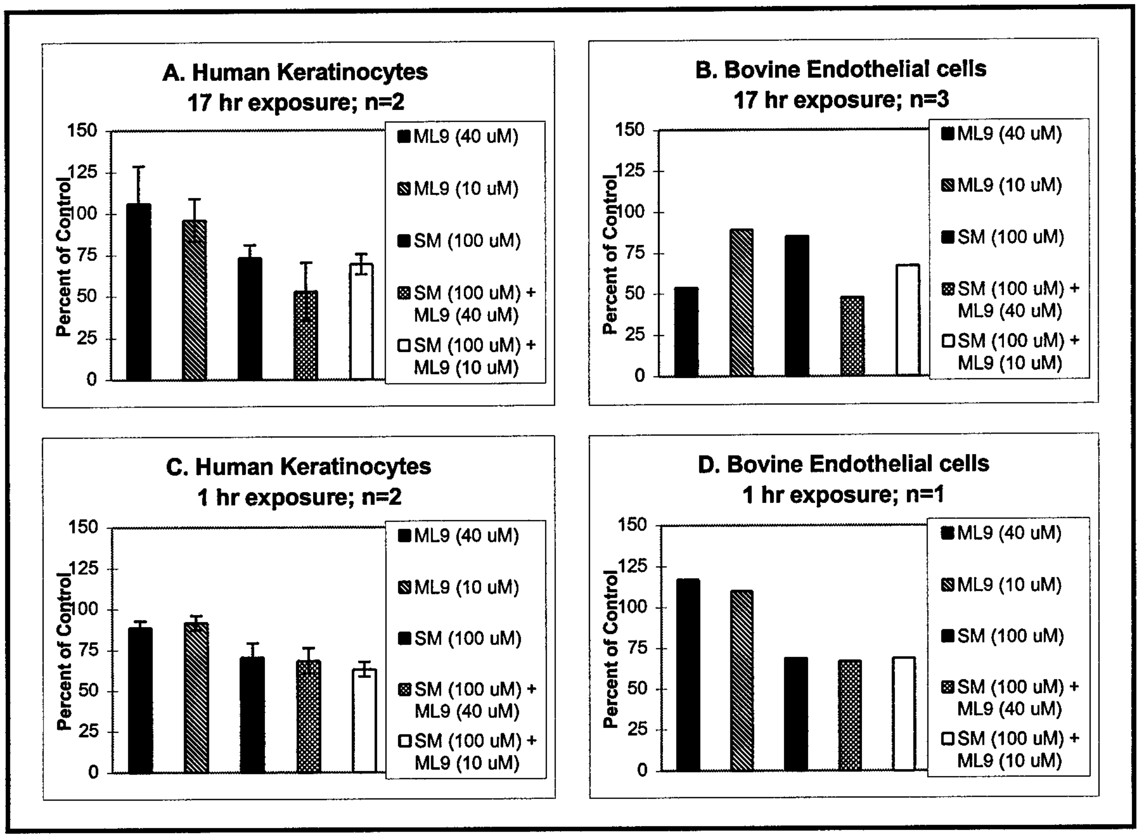
A. Human Keratinocytes
17 hr exposure; n=2
B. Bovine Endothelial cells
17 hr exposure; n=3
C. Human Keratinocytes
1 hr exposure; n=2
D. Bovine Endothelial cells
1 hr exposure; n=1
Percent of Control
0
25
50
75
100
125
150
■ ML9 (40 uM)
▨ ML9 (10 uM)
■ SM (100 uM)
▩ SM (100 uM) + ML9 (40 uM)
□ SM (100 uM) + ML9 (10 uM)

Fig. 7

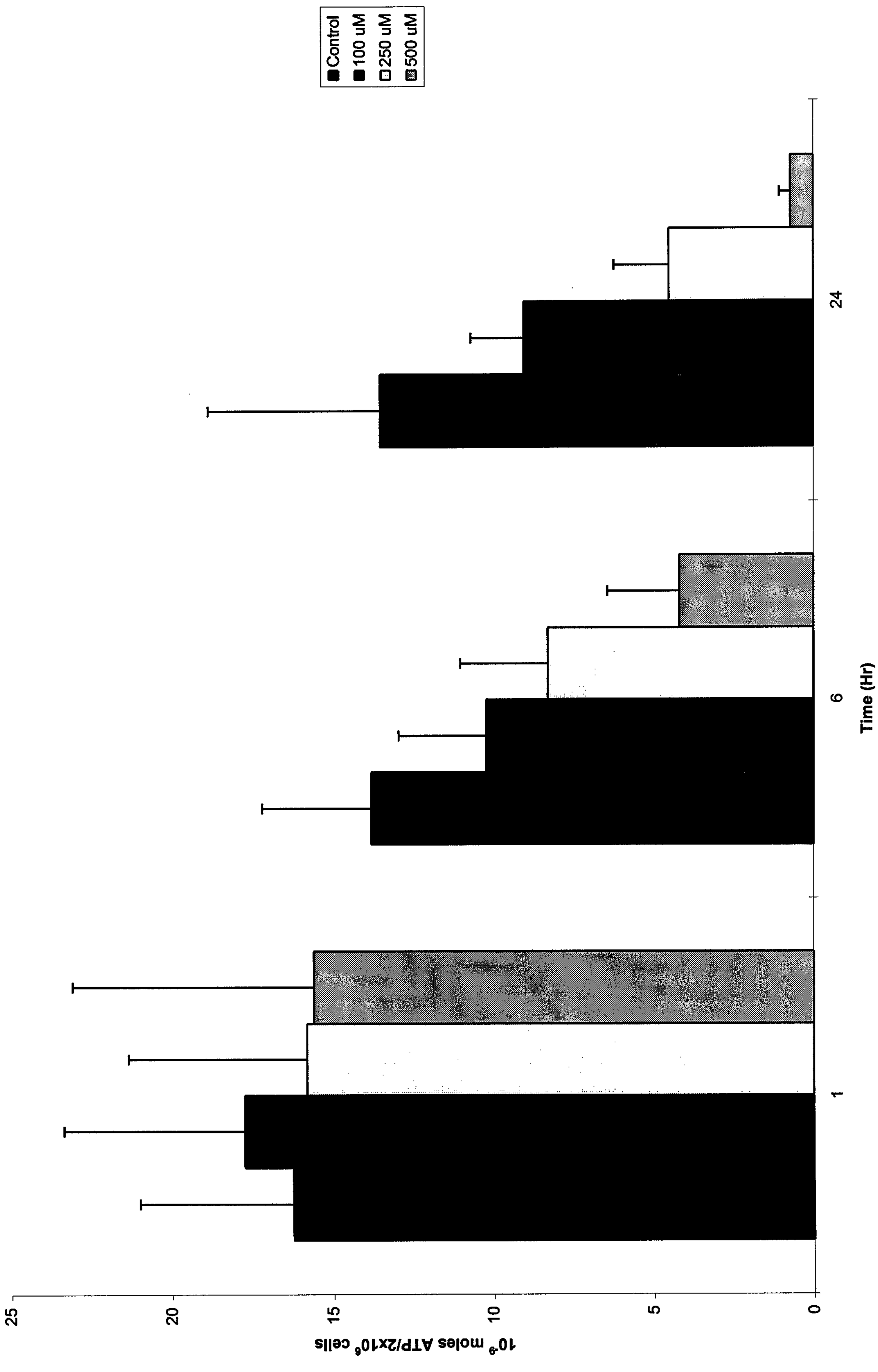

Control
100 uM
250 uM
500 uM
25
20
15
10
5
0
10^{-9} moles ATP/$2x10^6$ cells
1
6
24
Time (Hr)

Fig. 8A

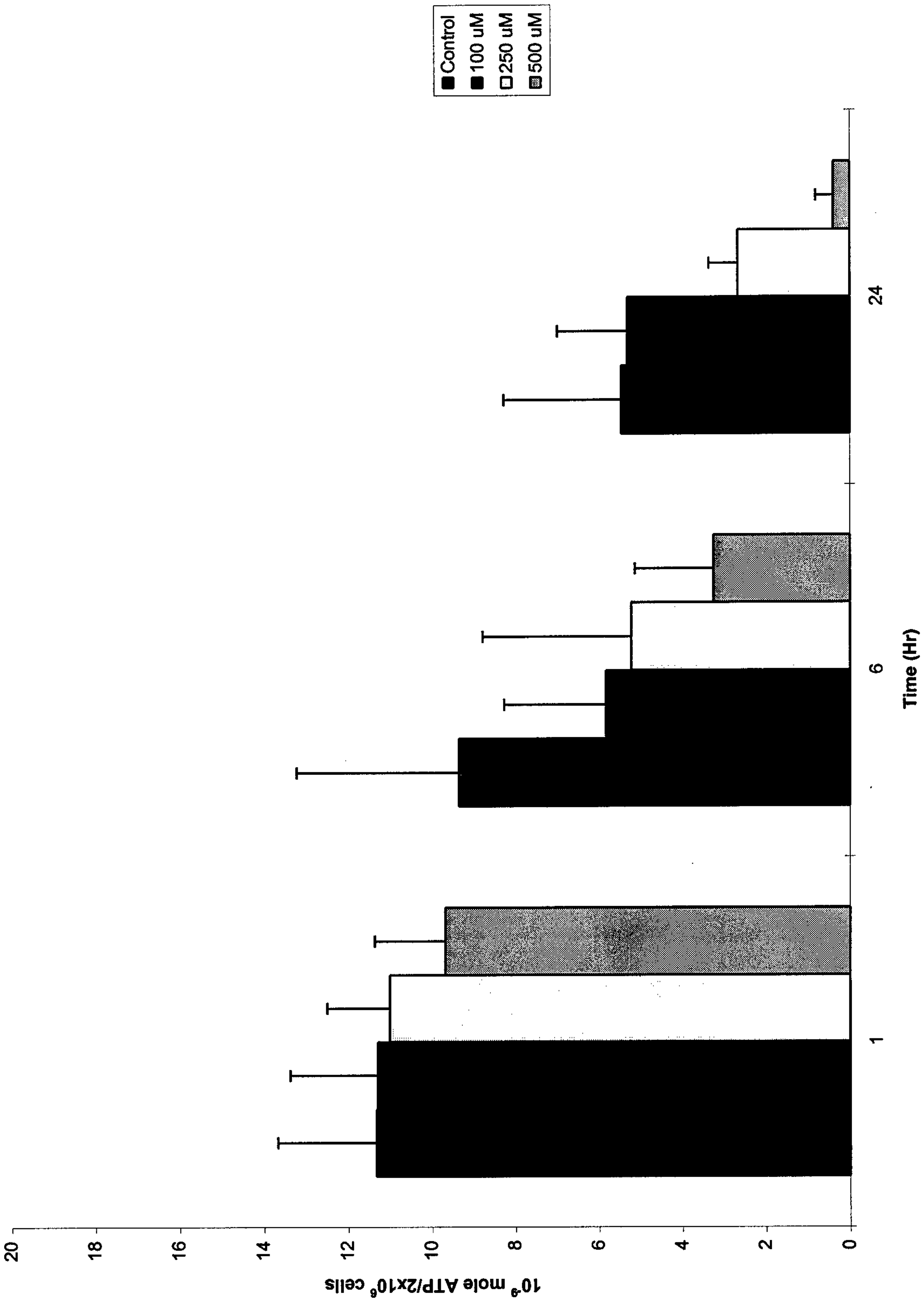
■ Control
■ 100 uM
□ 250 uM
▨ 500 uM
20
18
16
14
12
10
8
6
4
2
0
10-9 mole ATP/2x106 cells
1
6
24
Time (Hr)

Fig. 8B

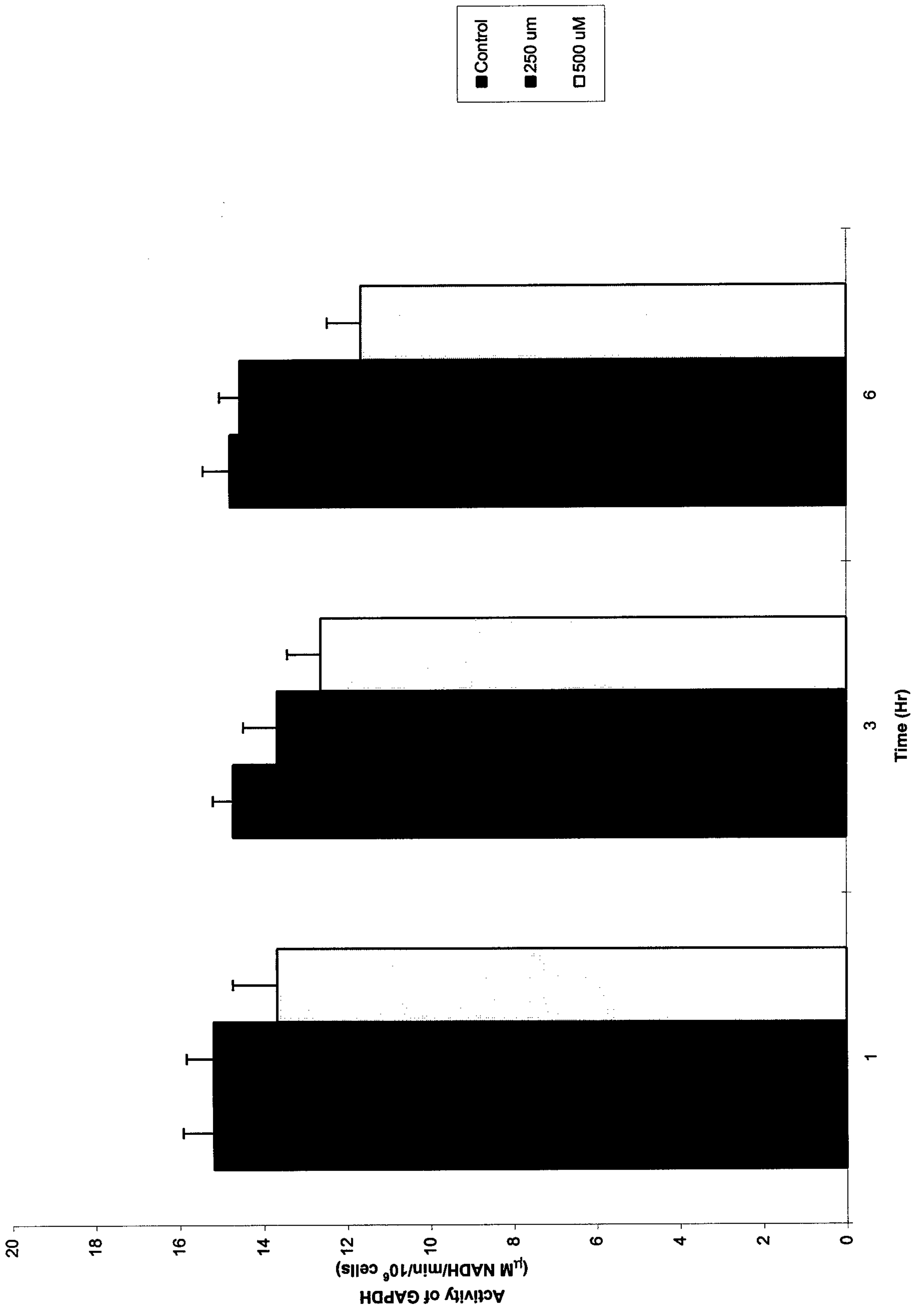
Activity of GAPDH
(μM NADH/min/10⁶ cells)
20
18
16
14
12
10
8
6
4
2
0
1
3
6
Time (Hr)
■ Control
■ 250 um
□ 500 uM

Fig. 9A

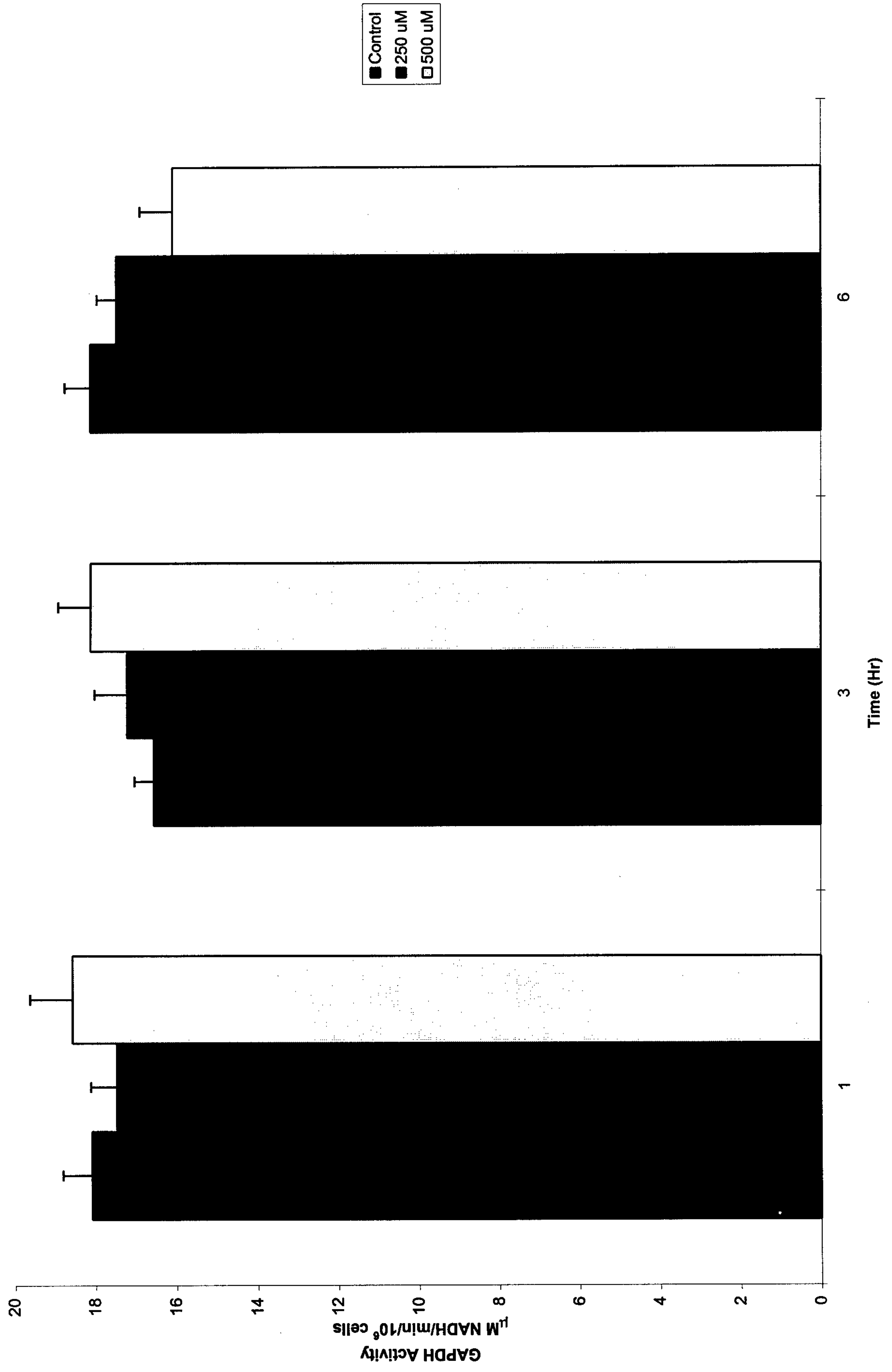

Control
250 uM
500 uM
GAPDH Activity
μM NADH/min/10⁶ cells
0
2
4
6
8
10
12
14
16
18
20
1
3
6
Time (Hr)

Fig. 9B

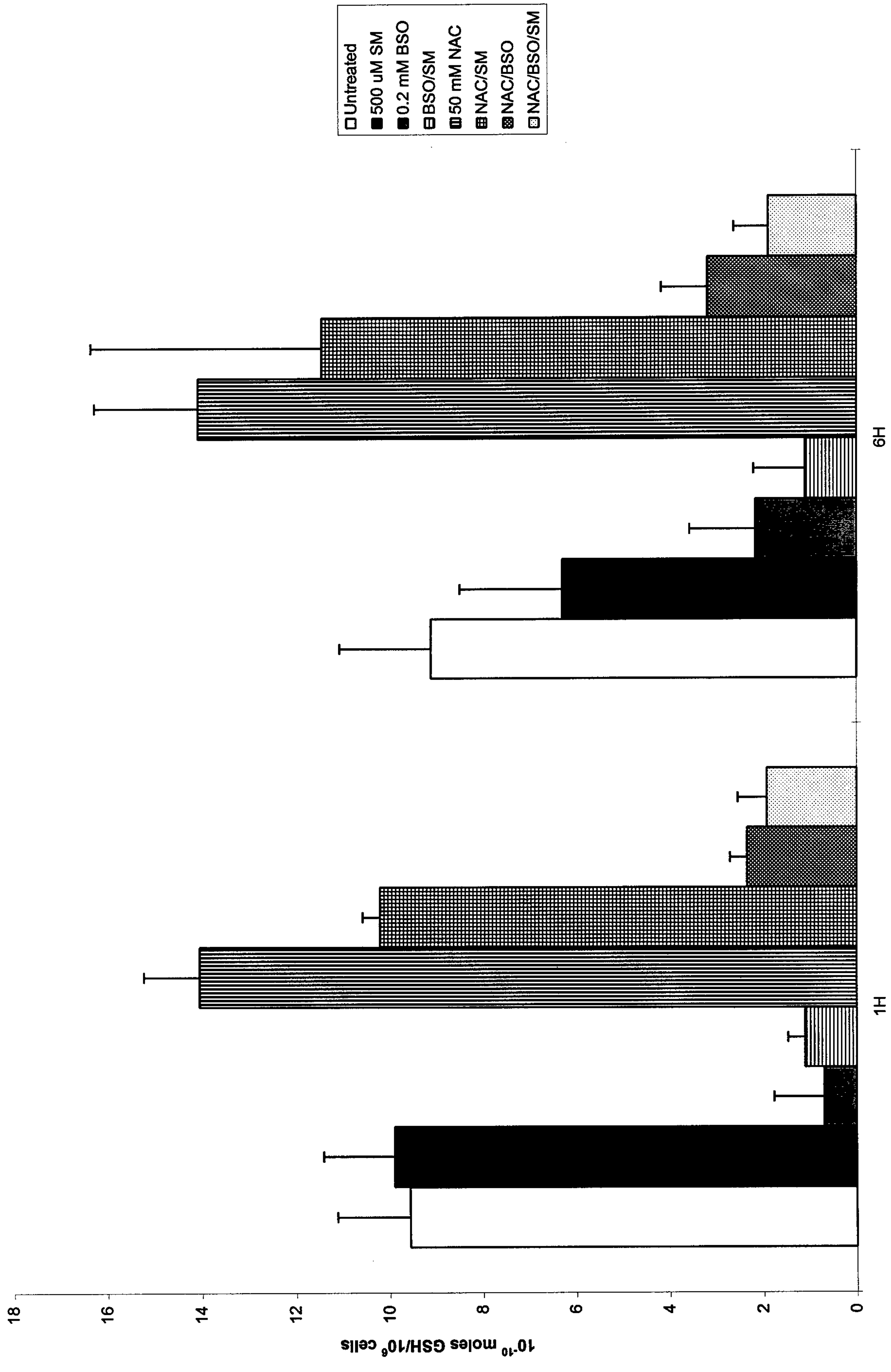

☐ Untreated
■ 500 uM SM
■ 0.2 mM BSO
▤ BSO/SM
▥ 50 mM NAC
▦ NAC/SM
▩ NAC/BSO
▨ NAC/BSO/SM
10-10 moles GSH/10^6 cells
0
2
4
6
8
10
12
14
16
18
1H
6H

Fig. 10A

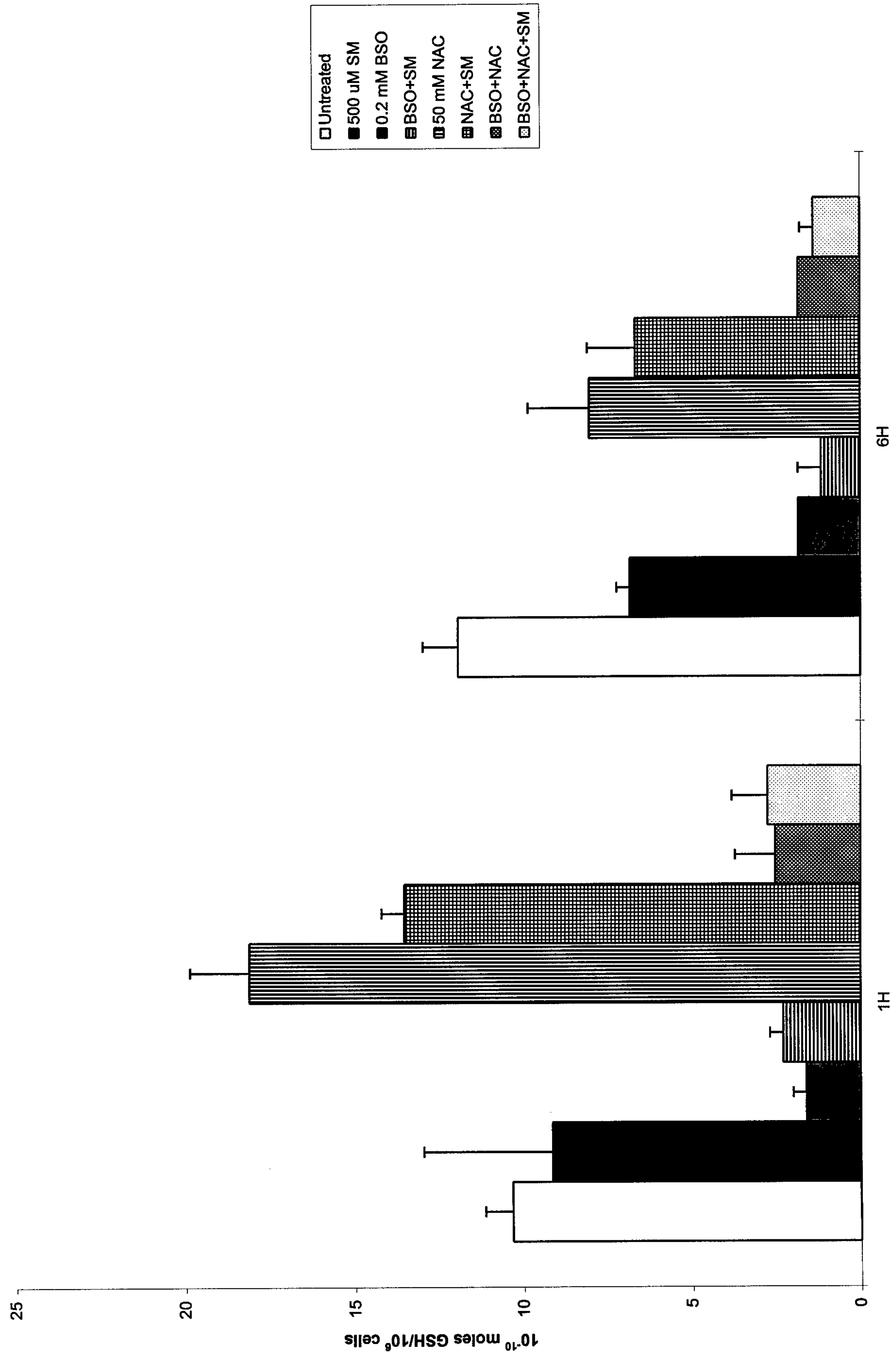

Untreated
500 uM SM
0.2 mM BSO
BSO+SM
50 mM NAC
NAC+SM
BSO+NAC
BSO+NAC+SM
10^{-10} moles GSH/10^6 cells
0
5
10
15
20
25
1H
6H

Fig. 10B

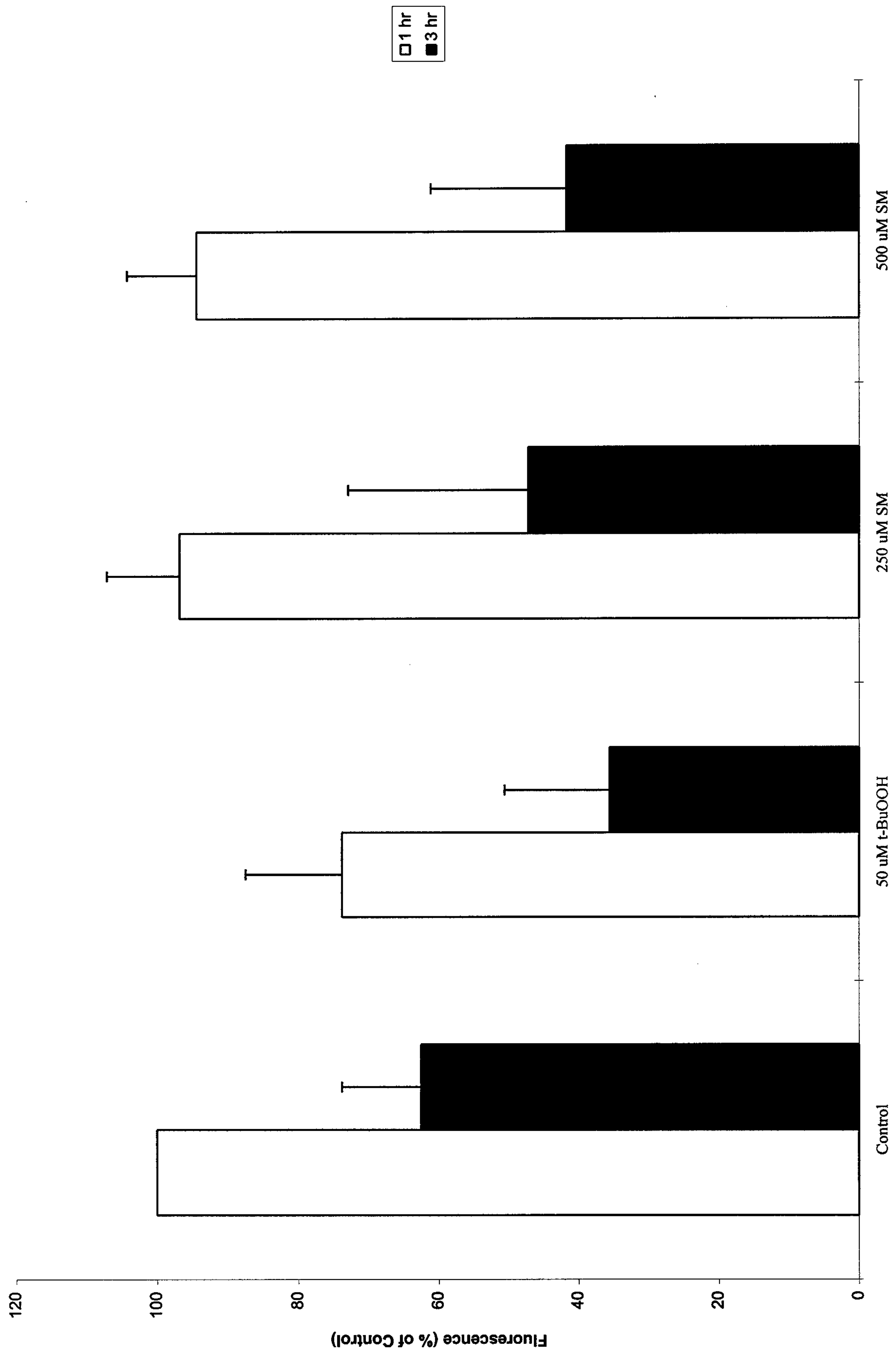

□ 1 hr
■ 3 hr
Fluorescence (% of Control)
0
20
40
60
80
100
120
Control
50 uM t-BuOOH
250 uM SM
500 uM SM

Fig. 11A

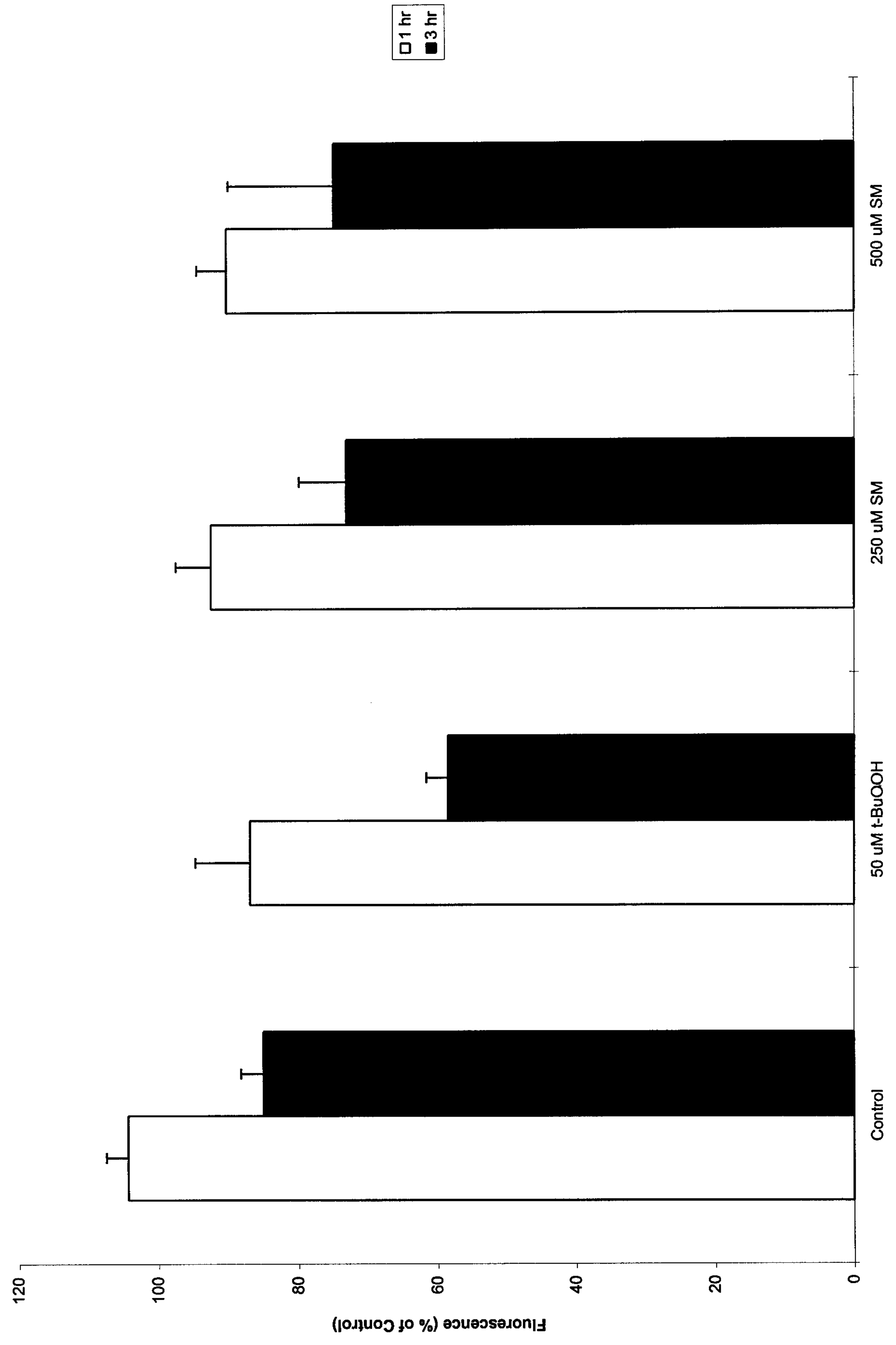

Fluorescence (% of Control)
0
20
40
60
80
100
120
Control
50 uM t-BuOOH
250 uM SM
500 uM SM
□ 1 hr
■ 3 hr

Fig. 11b

TOXICOLOGY AND APPLIED PHARMACOLOGY **141,** 568–583 (1996)
ARTICLE NO. 0324

Sulfur Mustard Induces Apoptosis and Necrosis in Endothelial Cells[1]

MILENA I. DABROWSKA, LAUREN L. BECKS, JOSEPH L. LELLI, JR., MINETTE G. LEVEE, AND DANIEL B. HINSHAW[2]

Departments of Surgery, VA Medical Center and University of Michigan, Ann Arbor, Michigan 48105

Received April 24, 1996; accepted July 25, 1996

Sulfur Mustard Induces Apoptosis and Necrosis in Endothelial Cells. DABROWSKA, M. I., BECKS, L. L., LELLI, J. L., JR., LEVEE, M. G., AND HINSHAW, D. B. (1996). *Toxicol. Appl. Pharmacol.* 141, 568–583.

Sulfur Mustard (SM) is a vesicant or blistering chemical warfare agent, for which there still is no effective therapy. Endothelial cells are one of the major cellular targets for SM. The mechanism of endothelial cell death during SM injury is poorly understood. We studied the effect of exposure of endothelial cells to 0–1000 μM SM over the time course of 2–24 hr to determine the role of apoptotic and necrotic patterns of cell death in endothelial injury induced by SM. SM concentrations ⩽250 μM induced exclusively apoptosis which was observed after 5 hr in 30% of endothelial cells. Exposure to SM concentrations ⩾500 μM caused apoptosis and necrosis to the same extent in 60–85% of all cells after 5 to 6 hr. Necrosis was accompanied by a significant (~50%) depletion of intracellular ATP, while in apoptotic cells ATP remained at the level similar to healthy cells. Interestingly, disruption of the long actin filament stress fibers and rounding of cells preceded other features of apoptosis—DNA fragmentation, membrane budding, and apoptotic body formation. In apoptotic cells, microfilaments formed constricted perinuclear bands, which were not observed in necrotic cells. Pretreatment with 50 mM N-acetyl-L-cysteine (NAC), a sulfhydryl donor and antioxidant, nearly eliminated the apoptotic features of cell death but did not prevent necrosis in response to SM. NAC pretreatment alone induced reorganization of actin filaments into an enhanced network of long stress fibers instead of a dominant cortical band of actin. NAC pretreatment prevented loss of cell adherence and cell rounding following exposure to 250 μM SM. The effect of NAC on cytoskeletal organization and its ability to eliminate SM-induced apoptosis suggests that actin filament organization may be an important element in cellular susceptibility to apoptotic stimuli. © 1996 Academic Press, Inc.

Sulfur mustard (SM) is a vesicant or blistering chemical warfare agent of historical and current interest (Smith *et al.,* 1995). There is still no effective treatment available to prevent or minimize injury induced by exposure to SM. Effective intervention will depend upon understanding the mechanism of action of this alkylating agent.

SM is a lipophilic compound which rapidly penetrates tissues, especially skin and the respiratory tract (Papirmeister *et al.,* 1991). Since SM penetration and therefore final tissue concentration closely depend on temperature and moisture as well as thickness of the epidermis (Papirmeister *et al.,* 1991), the effect of a broad range of SM concentrations is usually studied in *in vitro* experimental models (Rikimaru *et al.,* 1991). The major cellular targets involved early in the evolution of SM-induced skin lesions include keratinocytes and capillary endothelial cells. Up to the present, however, most of the studies have been focused on SM effects on keratinocytes (Momeni *et al.,* 1992; Papirmeister *et al.,* 1991; Vaughn *et al.,* 1988; Willems 1989).

In histological studies of human skin exposed to liquid SM, epithelial cell destruction appears to be primarily localized to the basal cell layer and the pattern of keratinocyte death appears to depend on the dose of SM (Ginzler and Davis, 1943). Formation of microblisters between the epidermis and dermis and loss of the epithelial layer have been observed only at intermediate (0.05–1 mM) concentrations of SM (Mitcheltree *et al.,* 1989; Mol *et al.,* 1991). When, concentration-related effects of SM have been examined in organ culture of full-thickness human skin explants (Rikimaru *et al.,* 1991), lower concentrations of the agent induced an increase in levels of histamine, plasminogen-activating activity, and prostaglandin E_2 as well as collagenase activity while at higher concentrations there was no increase in proteinase activity and less blister formation (Rikimaru *et al.,* 1991). The authors concluded that high concentrations of SM cause rapid necrosis thereby preventing any active response from the injured cells. Despite extensive studies of the SM effect on keratinocytes, the precise mechanism of cytotoxicity of this chemical warfare agent remains unknown.

Endothelial cells are considered to be another important cellular target of SM-mediated injury (Dannenberg *et al.,* 1985). It has been observed by others that an increase in vascular permeability is consistent with the cytotoxic damage caused by SM to capillaries in rabbit skin (Papirmeister

---

[1] This work is supported by the U.S. Army Medical Research and Material Command under Agreement No. 93-MM-3571 and also in part by the Department of Veterans Affairs. The views, opinions, and/or findings contained in this report are those of the authors and should not be construed as an official Department of the Army position, policy, or decision unless so designated by other documentation.

[2] To whom correspondence should be addressed at Surgery Service (112), VAMC, 2215 Fuller Road, Ann Arbor, MI 48105. Fax: (313) 769-7056.

0041-008X/96 $18.00
Copyright © 1996 by Academic Press, Inc.
All rights of reproduction in any form reserved.

et al., 1991). However, there are almost no data on the nature of endothelial cell injury induced by SM. The rapidity with which local edema may develop after SM exposure suggests that capillary leak which occurs as a result of the injury may not depend on actual endothelial cell necrosis but possibly on altered endothelial morphology (Papirmeister *et al.,* 1985). It was reported almost 50 years ago that after exposure to vesicant doses of SM, all of the endothelial cells underwent a form of karyorrhexis that the authors termed nuclear fragmentation (Friedenwald and Buschke, 1948). Therefore it is possible that the capillary leak which occurs as a result of SM injury may depend on active processes in cells that still have metabolic activity, a pattern of cell injury more like apoptosis (programmed cell death) then necrosis.

A great deal of interest and effort has been recently focused on understanding the nature of cell death, in the hope that the ability to regulate cell death may lead to new therapeutic modalities for a variety of conditions from cancer to inflammatory diseases. Cell death usually results via two morphologically and biochemically distinct pathways: necrosis (defined as "oncosis" by Majno and Joris (1995)) or apoptosis. Necrosis is the result of major perturbations in the cellular environment which result in failure of ATP generation or causes an increase in the permeability of the plasma membrane. This is accompanied by cellular and organelle swelling, membrane lysis, and leakage or spill of intracellular contents, resulting in secondary tissue damage through the induction of an inflammatory response. Apoptosis also leads to cell death, but in a slower manner which minimizes damage to neighboring cells. Early in the process, the plasma membrane ruffles, and the cell shrinks and rounds-up with a loss of cell–cell contact (Haake and Polakowska, 1993). Later, the cytoplasm and nuclear material condense, the DNA is broken down into multiples of the 180-bp nucleosomes, and the cell emits processes (the budding phenomenon). Finally, the whole cell separates into a number of membrane-bound vesicles containing intact organelles, termed apoptotic bodies, which then are removed by phagocytic cells. There is no spillage of proinflammatory material from the dying cells so apoptotic death occurs "silently" without acute inflammation (Schwartzman and Cidlowski, 1993). Apoptosis can be induced by a wide variety of stimuli, including physiologic and pathologic agents (Arends and Wyllie, 1991; Cohen, 1991; Martikainen *et al.,* 1990). It is still unclear whether apoptosis and necrosis are components of a common (overlapping) pathway of cell death or whether they represent two distinct phenomena (Hockenbery, 1995). Since it has been reported (Hockenbery *et al.,* 1993) that NAC (N-acetyl-L-cysteine) is able to block different models of apoptosis, we decided to use this tool to better define the apoptotic elements of cell death in our SM injury model.

The objective of this study was to determine the role of necrosis and apoptosis in the endothelial cell injury caused by SM exposure and the relationship of these two patterns of cell death to the morphological, cytoskeletal, and biochemical changes occurring in endothelial cells during the course of SM injury.

MATERIALS AND METHODS

Cells and culture. Bovine pulmonary artery endothelial cells were purchased from the National Institute of Aging, Aging Cell Culture Repository (Camden, NJ) and maintained in RPMI 1640 medium supplemented with 2 mM glutamine (GIBCO), 10% heat-inactivated fetal bovine serum (Whittaker, M.A. Bioproducts), 10 mM HEPES, 100 U/ml penicillin, and 100 mg/ml streptomycin (GIBCO). Cells were grown in 75- or 150-cm^2 flasks (Falcon) in a culture incubator at 37°C under a 5% CO_2 humidified atmosphere. Subculturing was carried out on confluent cultures using 0.05% trypsin and 0.02% EDTA (Sigma) and cells of Passages 3 to 7 were used.

Injury protocol with SM. Confluent monolayers of endothelial cells grown in six-well plates (Falcon, Becton Dickinson) were exposed to final concentrations of SM ranging from 0.01 to 1 mM in culture media under sterile conditions. Biochemical and morphological parameters of SM injury were monitored at multiple time points. Matched controls were also done over identical conditions and time points to which no SM had been added.

In the experiments in which cells were pretreated with N-acetyl-cysteine (NAC) to block apoptosis (Hockenbery *et al.,* 1993), the cells were incubated for 20 hr with 50 mM N-acetyl-L-cysteine (Sigma) (Hockenbery *et al.,* 1993). Residual NAC in the media was removed by three washings with media before SM addition.

Cell morphology. Microscopic observations of the endothelial cell monolayers were performed during the time course of SM injury with a Nikon optiphot microscope. Wright–Giemsa staining was performed using the Fisher LeukoStat Stain Kit. For better visualization of morphological details, photomicrographs of subconfluent monolayers were taken.

Determination of apoptotic index and cell viability (Duke and Cohen, 1992). Adherent endothelial cells grown in six-well plates were stained during the time course of SM injury with a dye mixture (10 μM acridine orange and 10 μM ethidium bromide; (Sigma), that was prepared in phosphate-buffered saline (PBS)).

Acridine orange (fluorescent DNA-binding dye) intercalates into DNA, making it appear green, and binds to RNA, staining it red–orange. Ethidium bromide is taken up only by nonviable cells, and its fluorescence overwhelms that of the acridine orange, making the chromatin of lysed cells appear orange.

At the end of each experimental time point, all of the medium was removed and cells were harvested by incubation with 0.05% trypsin and 0.02% EDTA for 1 min and washed with the medium. Then, 250 μl of cell suspension was mixed with 10 μl of the dye mix and 200 cells per sample were examined by fluorescence microscopy, according to the following criteria: (1) viable cells with normal nuclei (fine reticular pattern of green stain in the nucleus and red–orange granules in the cytoplasm); (2) viable cells with apoptotic nuclei (green chromatin which is highly condensed or fragmented and uniformly stained by the acridine orange); (3) nonviable cells with normal nuclei (bright orange chromatin with organized structure); and (4) nonviable cells with apoptotic nuclei (bright orange chromatin which is highly condensed or fragmented).

The study of the viability of cells in the undisturbed monolayers has shown that trypsinization does not promote further cell injury.

Measurement of endonucleolytic DNA cleavage (Laird et al., 1991). Cell samples (3×10^6 cells) obtained during the time course of SM injury were lysed in 750 μl of buffer (100 mM Tris, 5 mM EDTA, 200 mM NaCl, and 0.2% SDS at pH 8.5) to which Proteinase K (100 μg/ml final concentration) was added. Samples were incubated in a shaking water bath at 37°C for 1 hr. Then, DNA was precipitated by addition of an equal volume of cold isopropanol with gentle mixing. The precipitate was pelleted by centrifugation at 14,000g for 30 min, air dried (after decanting the supernatant) under a fume hood for 20 min, and then resuspended in 150 μl TE buffer (10 mM Tris, 1 mM EDTA, pH 7.6) containing 40 μg/ml RNase overnight at 25°C. Following the overnight incubation, 3 μl of the 10× loading buffer (0.25% bromophenol blue, 0.25% xylene cyanol FF, 30% glycerol) was added to 27 μl of the RNase-treated sample and 10 μl (~2 × 10^5 cells) was transferred to each well of a 1.6% agarose gel stained by 7 μg ethidium bromide. Horizontal agarose gel electrophoresis was performed at 120 mV for 1.5 hr. The gel was photographed under UV light.

ATP measurement. Cellular ATP levels were assayed as previously reported by the luciferase–luciferin method of Stanley and Williams (Hinshaw *et al.,* 1993). The luciferase–luciferin (Sigma) was reconstituted in a buffer containing 1% bovine serum albumin, 20 mM glycine, and 2 mM EDTA, pH 8.0. Measurements were performed in an LKB Model 1251 automated luminometer (LKB Instruments, Inc., Gaithersburg, MD). ATP data were expressed as nanomoles of ATP per 2 × 10^6 cells. The whole cell population, including floating cells, was subjected to the assay.

DNase I assay. The DNase I assay was used as previously described (Hinshaw *et al.,* 1991) for measurement of actin polymerization with the following modifications for adherent cells: cells grown to confluence in six-well plates were exposed to SM for variable periods of time. At the end of each experimental incubation, all of the medium in each well was removed and 1 ml of lysate solution containing 2 mM $MgCl_2$, 2 mM EGTA, 0.2 mM ATP, 0.5 mM dithiothreitol, 3% Triton X-100 (Tx-100), and 1 mM phenylmethylsulfonyl fluoride (PMSF) in Hanks' buffered salt solution was added to each well and pipetted 5 or 6 times to release all of the cells. Floating cells were also subjected to the assay. This was either immediately assayed for G-actin or added to an equal aliquot of a solution containing 1.5 M guanidine HCl, 1 M $NaCH_2CO_2$, 1 mM $CaCl_2$, 1 mM ATP, and 20 mM Tris–HCl, pH 7.5, mixed, and placed on ice for 20 min for later assay of total actin using the published method (Hinshaw *et al.,* 1991).

Fluorescence microscopy. After varying periods of incubation at 37°C under the different experimental conditions, the adherent cells were fixed with 2% paraformaldehyde for 1 hr at room temperature. The paraformaldehyde was then removed and the cells were washed and permeabilized three times for 5 min with Dulbecco's Cation Free PBS, pH 7.4, containing 0.2% Triton X-100. Cells were either stained with 165 nM rhodamine phalloidin (Molecular Probes) specific for F-actin in microfilaments (50) for 20 min at room temperature in the dark or exposed to a 1:50 dilution of antibody to tubulin within microtubules (1 mg/ml monoclonal mouse anti-β tubulin (Boehringer, Mannheim)) and then reacted with a rhodamine-conjugated anti-IgG to achieve visualization of the stained structures. Coverslips were sealed to each monolayer and the samples were viewed with the G filter block on a Nikon optiphot fluorescence microscope. Fluorescence micrographs were taken using TMAX 400 film (Kodak). For better visualization of morphological details, photomicrographs of subconfluent monolayers were taken.

Statistics. Analysis of variance (one-way ANOVA) and paired *t* tests were used for comparisons between experimental and control observations. Results are presented as means ± SEM for six to eight experiments unless otherwise noted.

RESULTS

SM Induces Apoptotic Morphology in Endothelial Cells

SM induced a reproducible morphological pattern of apoptotic changes in the endothelial cells over a 6-hr time course. Confluent control endothelial cells assumed multipolar or bipolar shapes and were well spread on the culture surface. Their nuclei showed a fine reticular pattern of chromatin and small, dark stained nucleoli (Fig. 1A). After 5 hr of SM exposure many cells shrunk, lost cell–cell contact, and exhibited nuclear chromatin condensation, plasma membrane budding, and formation of apoptotic bodies (Fig. 1B). Similar morphologic changes were seen also with other concentrations of SM tested (250 and 1000 μM) (data not shown).

In order to differentiate apoptotic from necrotic elements of cell injury induced by SM, confluent endothelial cells were pretreated with 50 mM NAC. NAC pretreatment of the endothelial cells was associated with distinct changes in the shape of the cells. The cells became more fusiform and spindle-shaped in comparison to the multipolar and more spread character of endothelial cells in their native state (Fig. 1C). After 5 hr of injury with 250 μM (data not shown) and 500 μM SM, the cells did not round and separate nor did they demonstrate "budding" and apoptotic body formation (Fig. 1D) as was observed in cells without NAC pretreatment (Fig. 1B). At the highest concentration of SM (1000 μM), the cells pretreated with NAC rounded but only a few of them (~5%) formed apoptotic bodies (data not shown).

The Effect of SM on the Pattern of Endothelial Cell Death

The determination of whether a cell dies by apoptosis as opposed to necrosis is most easily made on the basis of distinct structural changes in the cellular chromatin which occurs prior to the lysis of the plasma membrane. These changes include extensive condensation and fragmentation of the chromatin. The advantage of the assay we have used (Duke and Cohen, 1992) is the ability to potentially identify apoptotic nuclear features even in cells undergoing rapid plasma membrane lysis and necrosis through examination of changes in chromatin structure as well as membrane integrity (see the differentiating criteria under Materials and Methods).

The fluorescence microscopic assay of viability and apoptotic nuclear features described under Materials and Methods was used to evaluate the effect of a range (0–1000 μM) of SM concentrations over a 6-hr time course on the viability of adherent endothelial cells. SM at these concentrations induced apoptosis during the 6-hr time course (Fig. 2A). At 3 hr after exposure to these concentrations of SM only a small percentage of apoptotic cells (5–8%) was observed, which increased significantly at later time points (after 5 or 6 hr). After 6 hr, a significant number of apoptotic cells (19%) was visible even with 100 μM SM, and after 24 hr the percentage of apoptotic cells became even more prominent (~50%) (data not shown). The higher concentrations of SM (500 and 1000 μM) induced apoptosis and necrosis to a similar extent in the injured endothelial cells and induced loss of cellular adherence (Fig. 2A). Necrosis induced by the higher concentrations of SM tended to develop more rapidly than apoptosis. The 1000-μM concentration of SM induced significant increases in the percentage of necrotic adherent cells as early as 3 hr after SM exposure. After exposure to 500 μM SM, the percentage of necrotic cells which remained adherent was very small after 6 hr (Fig. 2A). The loss of endothelial cell adherence resulting in the appearance of floating cells (80% of these cells were necrotic; 20% apoptotic) was clearly noticeable at 5 and 6 hr after exposure to 500 μM SM. One thousand micromolar SM produced greater numbers of floating cells, ~20% and 30%, respectively, at 5 and 6 hr. This loss of cell adherence may explain the paradoxically lower percentage of apoptotic and especially necrotic cells at the later time points. Pretreatment with NAC largely prevented cellular apoptosis as well as the appearance of floating cells (Fig. 2B). Interestingly, necrotic cell numbers remained at the level observed for cells not pretreated with NAC (see total number of necrotic and floating cells in Fig. 2A).

Time- and Dose-Dependent Effects of SM on Endothelial DNA

To confirm the morphologic evidence of nuclear fragmentation, DNA was extracted and analyzed with agarose gels. The DNA "ladder" of multiples of the 180-bp nucleosomes, characteristic for endonucleolytic cleavage of DNA during apoptosis, was clearly detected in SM-injured cells after 5 and 6 hr in all tested concentrations of SM. The DNA fragmentation was not visualized at time points earlier than 3 hr. DNA from control cells remained intact throughout the 6-hr time course (Fig. 3). The characteristic DNA ladder was not demonstrable throughout the time course of SM injury with NAC pretreatment except for a faint ladder with 1000 μM SM at 6 hr (Fig. 3).

The Effect of SM on Intracellular ATP Levels

Reductions in ATP levels are often features of cellular injury leading to necrosis. Measurement of ATP levels in endothelial cells after SM injury revealed significant reduction of ATP levels only in cells treated with 500 and 1000 μM SM (Fig. 4A). There was a significant decrease (⩾30%) from the control intracellular ATP level ($p < 0.05$) with both concentrations as early as 3 hr after SM exposure. Later in the course of SM injury (6 hr) further depletion of cellular ATP was seen to 33 or 11% of control values in cells subjected to 500 or 1000 μM, respectively (Fig. 4A). The reduction in ATP associated with these higher concentrations of SM correlated well with the loss of cellular adherence and the high percentage of dying cells.

Pretreatment with 50 mM NAC largely prevented the decrease in intracellular ATP levels induced by SM concentrations ⩾500 μM at 3 and 5 hr (Fig. 4B). Later (after 6 hr) in the course of injury with SM concentrations ⩾500 μM, ATP levels were decreased ($p < 0.05$). However, these reductions (to ~50%) were not as dramatic as in cells injured by SM without NAC pretreatment (Fig. 4A).

The Effect of SM on G-actin Content in Endothelial Cells

Because changes in cellular levels of polymerized or filamentous (F)-actin may be of central importance to the morphologic changes of apoptosis (Hinshaw *et al.,* 1986) and may account for changes in the intensity of staining with rhodamine–phalloidin, we quantitated average changes in monomeric G-actin as an indirect measure of F-actin (F-actin = Total actin − G-actin). Monomeric (G)-actin as a percentage of total cellular actin was measured at 2 hr (early in the course of morphological changes in the cells) and 6 hr after SM exposure (when apoptotic body formation is clearly visible in a large percentage of cells). SM at the highest concentration (1000 μM) caused an initial decrease in G-actin (actin polymerization) at a time (2 hr) which preceded the onset of major apoptotic changes in cellular morphology (budding and DNA fragmentation) and loss of adherence (Fig. 5). Lower concentrations of SM (250 and 500 μM) were not associated with significant differences in G-actin content as a percentage of total actin. At a later time point (6 hr), a significant increase in G-actin as a percentage of total actin (actin depolymerization) was observed in cells exposed to 1000 μM SM (Fig. 5).

The Effect of SM on Cytoskeletal Organization in Endothelial Cells

Since morphological changes which occur in the course of apoptosis or necrosis may result from cytoskeletal reorganization, we studied the effect of SM on microfilament and microtubule organization, major cytoskeletal determinants of cellular morphology. Fluorescence micrographs of endothelial cells were taken after cellular fixation and staining of F-actin within microfilaments with rhodamine–phalloidin at different times after SM injury. Control cells demonstrated a prominent cortical band of microfilaments as well as many thin, elongated stress fibers located at the periphery of the cells (Fig. 6A). After SM injury, the cells began to round up and separate from each other so that prominent gaps were seen between the cells (Fig. 6B). Localization of F-actin revealed that, in the course of SM injury, the long stress fibers gradually disappeared (Figs. 6B and 6C), while the peripheral cortical band of microfilaments decreased in size but remained present in the major part of the cell population in a perinuclear location (Fig. 6C). Since at 5 hr after 1000 μM SM injury ~70% of attached cells were apoptotic, the presence of the perinuclear

FIG. 1. Micrographs of Wright–Giemsa-stained endothelial cells as described under Materials and Methods. (A) Control endothelial cells. (B) Cells exposed to 500 μM SM, after 5 hr. (Arrow) chromatin condensation. (C) Control endothelial cells pretreated with NAC. Note the elongated, more fusiform shape of the cells. (D) Cells pretreated with NAC and exposed to 500 μM SM, after 5 hr. Bar is equivalent to 20 μm.

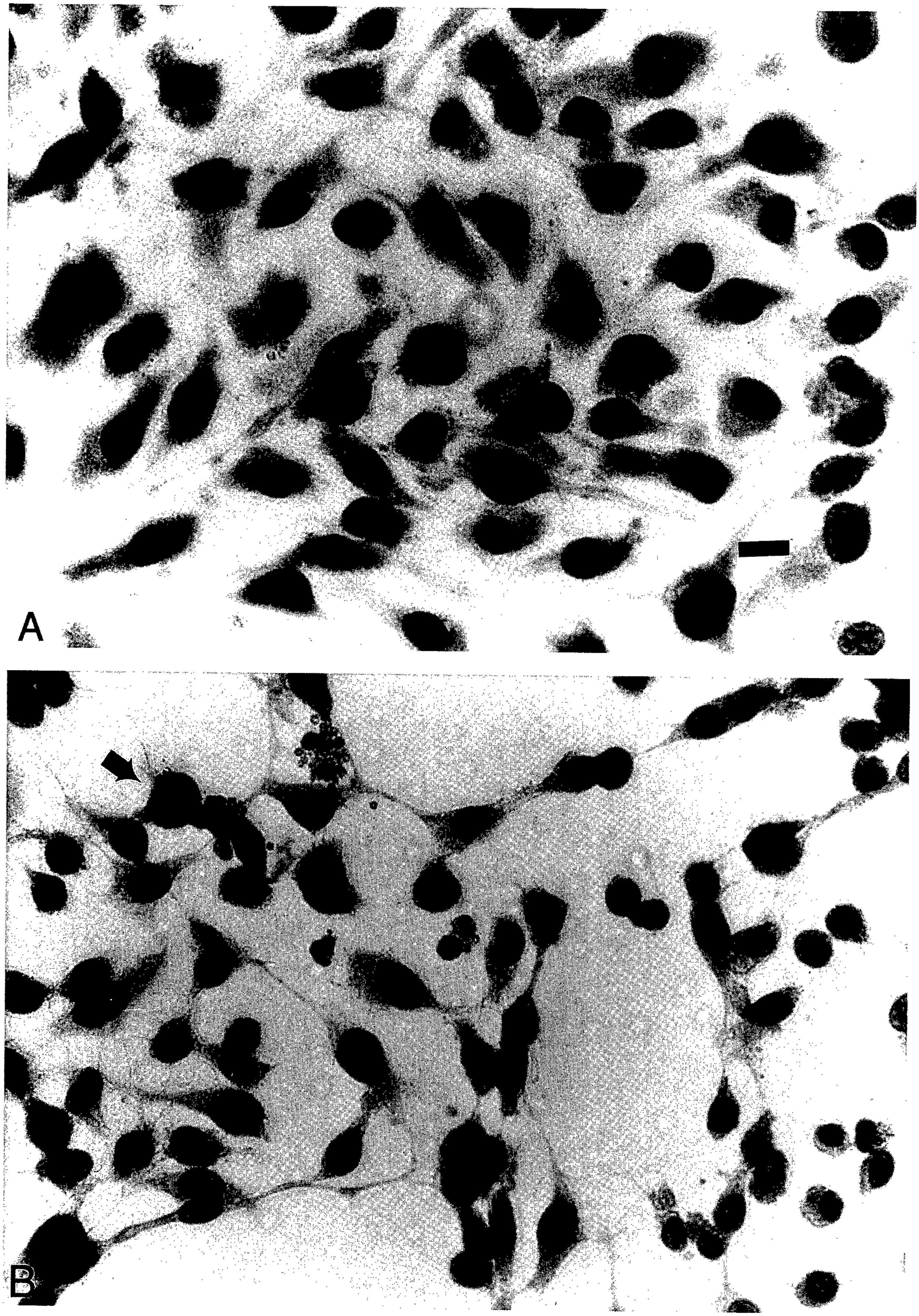
A
B

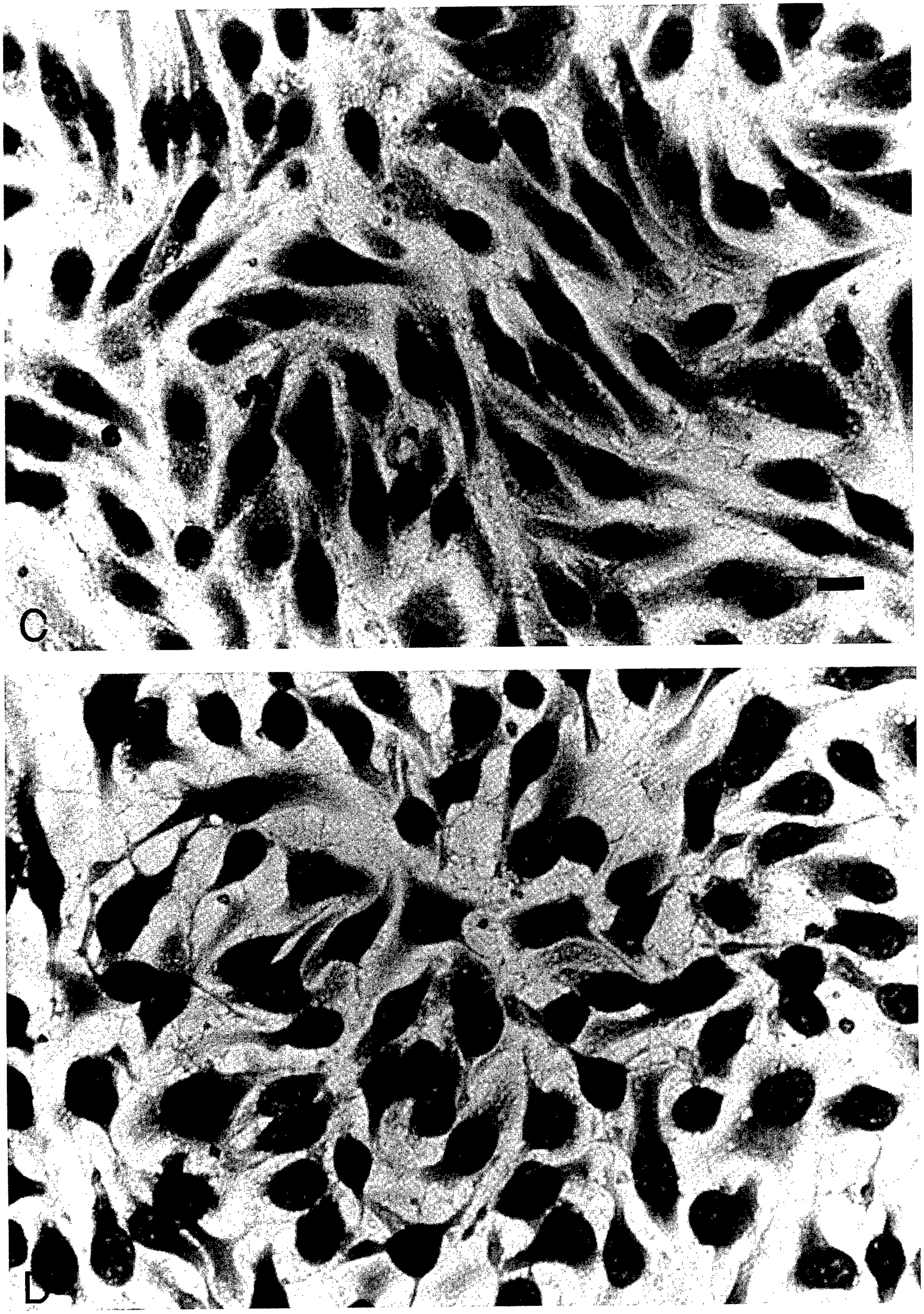

FIG. 1—*Continued*

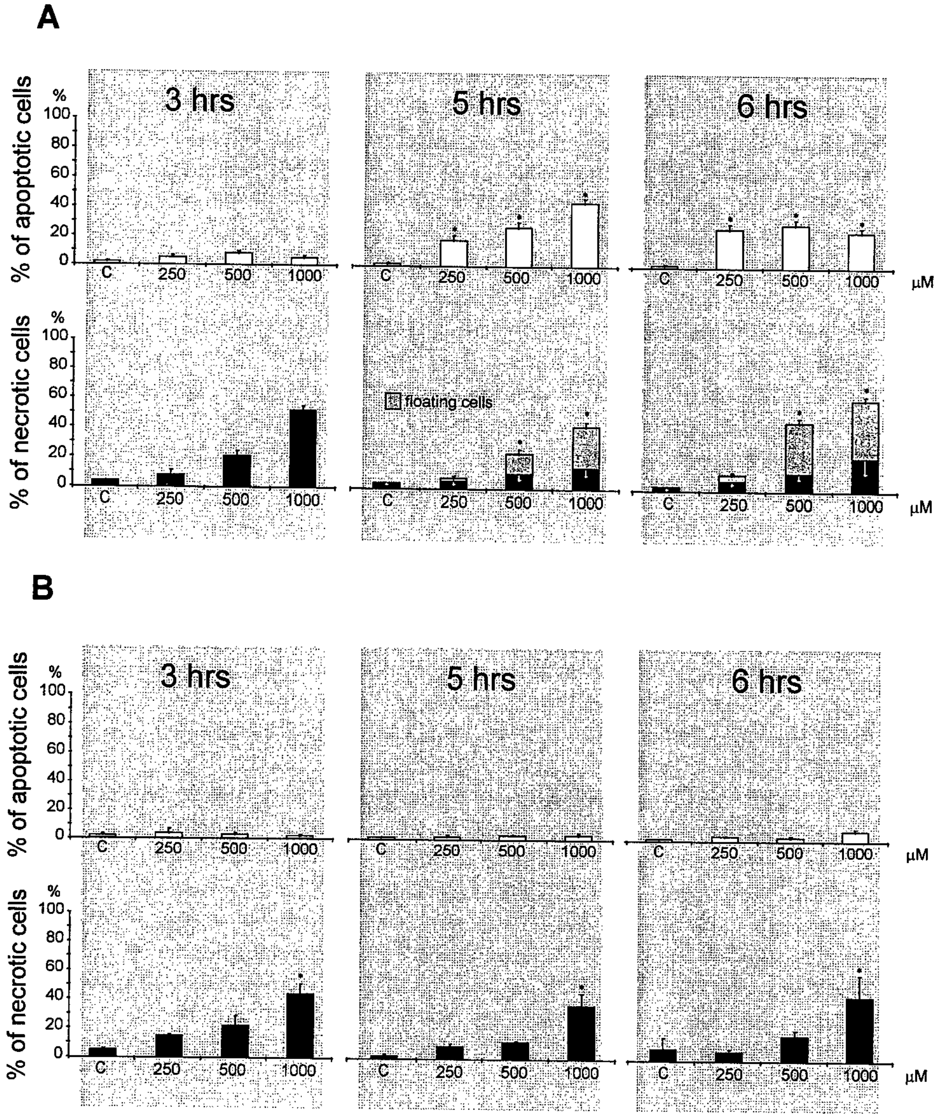

FIG. 2. Viability of adherent endothelial cells after exposure to different concentrations of SM over a 6-hr time course, without (A) and with (B) NAC pretreatment. Each bar represents the mean percentage of six separate experiments ±SEM. Asterisks indicate statistically significant differences ($p \leq 0.05$; one-way ANOVA) compared to corresponding control. Apoptotic and necrotic cells were differentiated according to criteria described under Materials and Methods. Percentage of viable nonapoptotic cells, 100%-[Apoptotic(%) + Necrotic(%) + Floating(%) cells]; floating cells, cells which had lost adherence (~80% of these cells were necrotic, ~20% apoptotic). Note the dramatic difference in percentage of apoptotic and floating (0%) cells in B compared to A.

actin band may be a pathologic feature unique to the apoptotic mode of endothelial cell death.

Control cells pretreated with NAC showed, instead of a prominent cortical band of actin (Fig. 6A), a complex network of long stress fibers (Fig. 6D). After 5 hr of injury, stress fibers were still present in cells exposed to 250 μM (data not shown) and 500 μM SM and the majority of the cells did not round up and separate from each other to the extent seen without NAC pretreatment (compare Fig. 6E with Fig. 6B). Consistent cellular rounding was observed only at 1000 μM SM (Fig. 6F). In the majority of cells (~90%) we could not find the centrally located perinuclear bands of actin, only globular fragments of actin filaments were observed in the dying cells.

The Effect of SM on Microtubule Organization in Endothelial Cells

Control cells stained for β-tubulin in microtubules demonstrated a normal pattern of microtubules radiating from the microtubule-organizing center, lying just outside the nucleus (Fig. 7A). After SM injury, the microtubules depolymerized

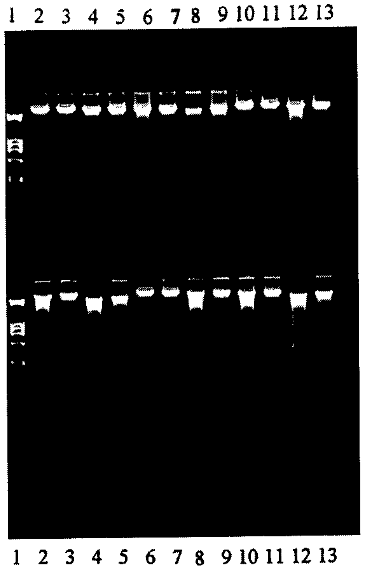

FIG. 3. Agarose gel electrophoresis of DNA extracted from endothelial cells. Lanes 1, DNA molecular size marker (*Hin*dIII/*Hae*III; GIBCO). Top, lanes 2, control cells, at 3 hr; 3, control cells pretreated with NAC, at 3 hr; 4, cells exposed to 250 μM SM, at 3 hr; 5, cells pretreated with NAC and treated with 250 μM SM, at 3 hr; 6, cells exposed to 500 μM SM, at 3 hr; 7, cells pretreated with NAC and treated with 500 μM SM, at 3 hr; 8, cells exposed to 1000 μM SM, at 3 hr; 9, cells pretreated with NAC and treated with 1000 μM SM, at 3 hr; 10, control cells, at 5 hr; 11, control cells pretreated with NAC, at 5 hr; 12, cells exposed to 250 μM SM, at 5 hr; 13, cells pretreated with NAC and treated with 250 μM SM, at 5 hr. Bottom, lanes 2, cells exposed to 500 μM SM, at 5 hr; 3, cells pretreated with NAC and treated with 500 μM SM, at 5 hr; 4, cells exposed to 1000 μM SM, at 5 hr; 5, cells pretreated with NAC and treated with 1000 μM SM, at 5 hr; 6, control cells, at 6 hr; 7, control cells pretreated with NAC, at 6 hr; 8, cells exposed to 250 μM SM, at 6 hr; 9, cells pretreated with NAC and treated with 250 μM SM, at 6 hr; 10, cells exposed to 500 μM SM, at 6 hr; 11, cells pretreated with NAC and treated with 500 μM SM, at 6 hr; 12, cells exposed to 1000 μM SM, at 6 hr; 13, cells pretreated with NAC and treated with 1000 μM SM, at 6 hr. Note the lack of "ladders" throughout the time course after NAC pretreatment except for a faint "ladder" with 1000 μM SM, at the late time point of 6 hr.

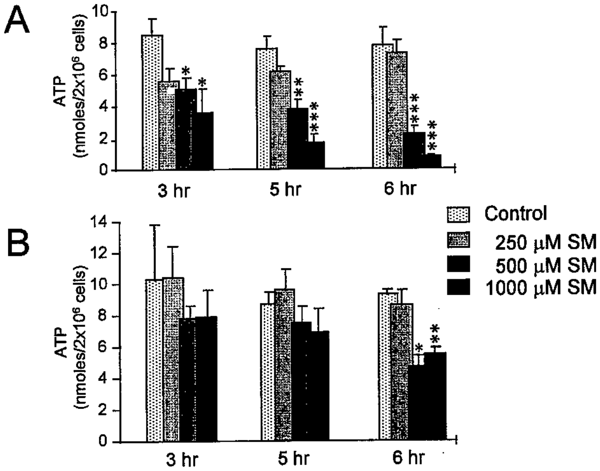

FIG. 4. The effect of SM (0–1000 μM) on ATP levels in endothelial cells over a 6-hr time course. Each bar represents the mean + SEM of $N = 6$ separate experiments. $^*p < 0.05$; $^{**}p < 0.005$; $^{***}p < 0.001$; *t* test (SM versus control). (A) Cells without NAC pretreatment; (B) cells pretreated with NAC.

during the 5-hr time course only at high concentrations of SM (Fig. 7B). NAC pretreatment had no effect on microtubule organization in uninjured endothelial cells and did not prevent tubulin depolymerization in response to SM injury (data not shown).

Endothelial Cell Adherence during the Course of SM Injury

The appearance of floating cells after exposure to higher concentrations of SM (see Fig. 2A) suggested that SM injury decreases cellular adherence. The effect of SM on endothelial cell adherence was measured by trypsinizing and counting cells which remained adherent after SM injury. SM at the 250-μM concentration did not cause a decrease in the number of adherent cells as late as 6 hr after SM exposure (Fig. 8A). Higher concentrations of SM (500 and 1000 μM) induced significant loss of adherent cells at later time points (at 6 and even at 5 hr, respectively) (Fig. 8A). These data correlate very well with the appearance of floating cells (see Fig. 2). In cells pretreated with NAC, the number of adherent cells did not change during the time course with all concentrations of SM tested (Fig. 8B).

DISCUSSION

Our evaluation of cellular morphology, viability, and biochemical parameters revealed, for the first time, that SM induces apoptotic or apoptotic/necrotic patterns of endothelial cell death. After 5 hr of injury, 250 μM SM induced features typical for apoptosis. At lower concentrations these

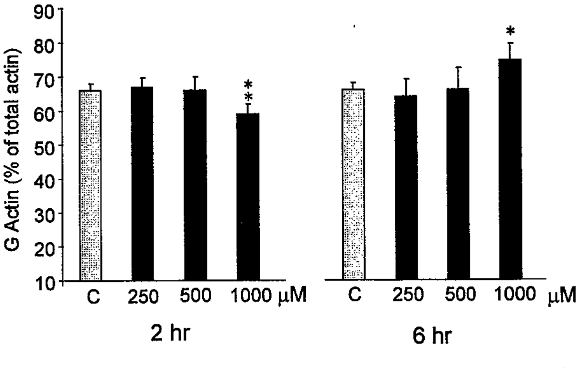

FIG. 5. DNase I measurement of changes in actin within SM-injured endothelial cells. Each bar represents the mean + SEM of $N = 4$ or 5 separate experiments performed in triplicate. $^*p < 0.05$; $^{**}p < 0.03$; *t* test (SM versus control).

features were clearly observed after 24 hr. Higher concentrations (≥500 μM) of this agent caused rapid necrosis observed by 3 hr; however, after 5 hr apoptosis was also present in part of the cell population. The DNA "ladder" characteristic for endonucleolytic cleavage of DNA during apoptosis was clearly detected by 5 hr after exposure to concentrations of SM ≥250 μM. Since necrosis, caused by higher concentrations of SM, was also accompanied by apoptosis, the type of endothelial cell death caused by SM appeared to not be entirely dose dependent. Variations in the apoptotic or necrotic response to injury may depend on individual differences in cell cycle and metabolism (Bursch, 1990).

Pretreatment of endothelial cells with NAC nearly eliminated the apoptotic pathway of cell death in response to SM and significantly increased the number of non-apoptotic viable cells. This was also confirmed by agarose gel analysis of DNA isolated from SM-injured endothelial cells, since the DNA "ladder" was not demonstrable in cells pretreated with NAC except for the highest concentration of SM. At the same time NAC did not prevent the necrotic pathway of cell death which suggests that SM may induce apoptosis and necrosis in endothelial cells via different mechanisms. Therefore, our observations support the hypothesis that apoptosis and necrosis are distinct pathways of cell death (Hockenbery, 1995). Experimental models dealing with this problem have been difficult to interpret since overexpression of the proto-oncogene bcl-2 (used as a tool for inhibition of apoptosis) has been associated with cellular protection from apoptosis as well as necrotic cell death (Kane *et al.,* 1993; Reed, 1994; Zhong *et al.,* 1993).

The beneficial effect of NAC treatment on SM-induced cytotoxicity has been reported in human peripheral blood lymphocytes (Cowan *et al.,* 1992) and basal cells (Zhang *et al.,* 1995). It has been suggested that NAC treatment interferes with free radical formation via different mechanisms, possibly working directly as a free radical scavenger, as a precursor of reduced glutathione (GSH) via its function as a "thiol supplier" or as a structural analogue of glutathione enriching the GSH pool in the cellular environment (De Flora and De Vries, 1993; Malorni *et al.,* 1993). Depletion of GSH content sensitized lymphocytes to SM (Gross *et al.,* 1993), whereas cysteine protects cells from SM cytotoxicity (Burgunder *et al.,* 1989; Meister *et al.,* 1986). Therefore elimination of apoptosis by NAC pretreatment suggests that endothelial cell apoptosis may be linked with oxidative stress. This mechanism of SM toxicity has also been suggested by others (Papirmeister *et al.,* 1991; Smith *et al.,* 1995), although further studies are necessary to confirm this hypothesis.

Metabolic Effect of SM Injury

Several investigations have focused on the alkylating properties of SM and impairment of energy metabolism by this agent (Papirmeister *et al.,* 1991). One theory of SM cytotoxicity proposes the following sequence: (1) SM alkylates purines in DNA leading to (2) activation of the chromosomal enzyme-poly(ADP-ribose)polymerase finally resulting in (3) depletion of NAD^+ and inhibition of ATP synthesis (Meier *et al.,* 1987). It was found, that decreases in NAD^+ levels preceded and were correlated with the predicted severity of the toxic effects. On the other hand, many authors have reported a lack of correlation between maintenance of NAD^+ levels and cell death or microvesicle formation after SM injury (Mol *et al.,* 1989; Yourick *et al.,* 1991). We found that concentrations of SM ≥500 μM caused progressive decreases in endothelial ATP levels which were accompanied by loss of cell viability (especially necrosis) and adherence. In cells pretreated with NAC, ATP levels were only slightly decreased early in the course of SM-induced injury and only after 6 hr of exposure to high concentrations of SM were they significantly depleted. Interestingly, 250 μM SM, which only induced the apoptotic pathway of cell death, did not cause substantial reduction of the intracellular ATP level. Therefore, in endothelial cells, SM-induced impairment of ATP synthetic pathways may play an important role in SM-induced necrosis, but not apoptosis.

The Effect of SM on the Endothelial Cytoskeleton

In endothelial cells undergoing SM-induced apoptosis, cytoskeletal reorganization preceded other features of this form of cell death—DNA fragmentation, cell membrane blebbing, and apoptotic body formation. This suggests that cytoskeletal reorganization may represent one of the earliest cellular responses to SM injury. Cytoskeletal reorganization as evidenced by rounding of adherent endothelial cells and changes in polymerized actin was clearly visible as early as 2 hr after exposure to ≥500 μM SM. Previous data have shown, that oxidizing conditions are correlated with assembly of polymerized actin and that this represents a biochemical process that is distinct and separate from the ATP-dependent disruption of visible microfilament organization (Hin-

FIG. 6. Fluorescence micrographs of rhodamine phalloidin-stained endothelial cells as described under Materials and Methods. (A) Control cells; (B) cells exposed to 500 μM SM, after 2 hr; (C) cells exposed to 1000 μM SM, after 5 hr. Note the thinning and loss of stress fibers and the apparent shrinkage/contraction of the peripheral (cortical) band of actin filaments (arrows) which correlates well with cell shrinkage (bar is equivalent to 20 μm); (D) control endothelial cells pretreated with NAC; (E, F) cells pretreated with NAC and exposed to 500 and 1000 μM SM, respectively, after 5 hr. Note the extensive network of long stress fibers in control cells and their reduced but still visible presence after injury (Fig. 6E). Also note the absence of perinuclear rings of actin at all concentrations of SM tested (e.g., F). Bar is equivalent to 20 μm.

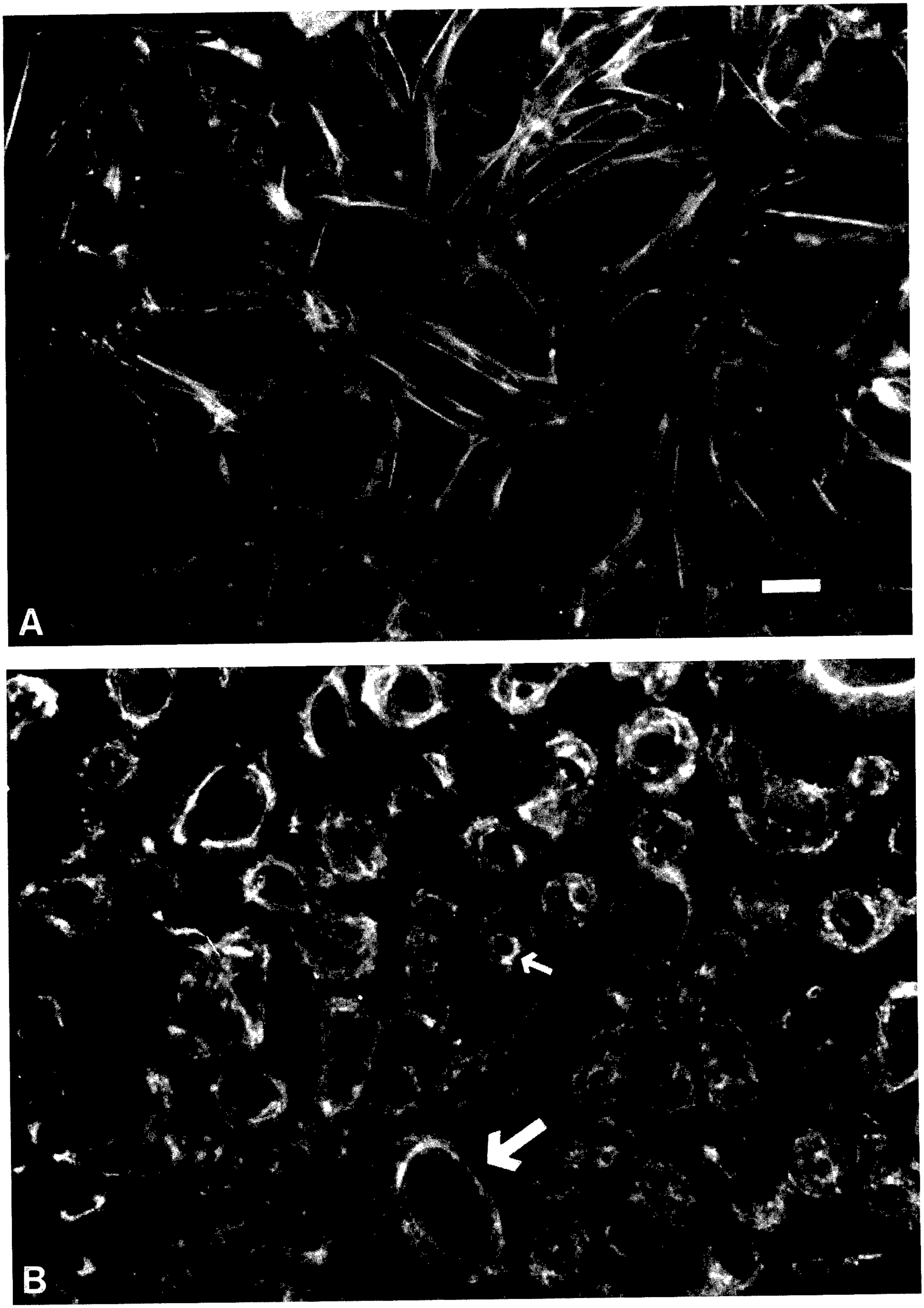
A
B

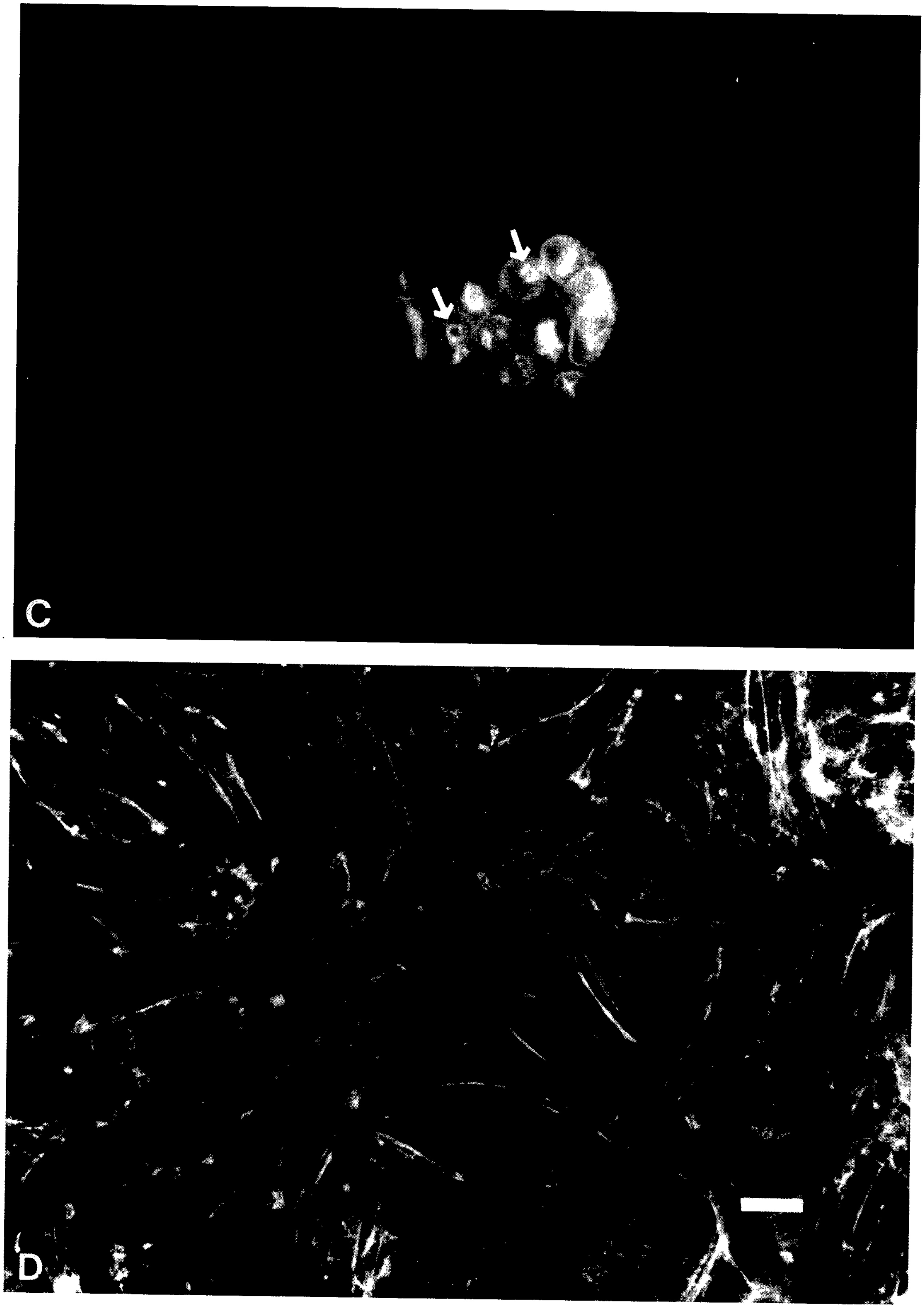

FIG. 6—*Continued*

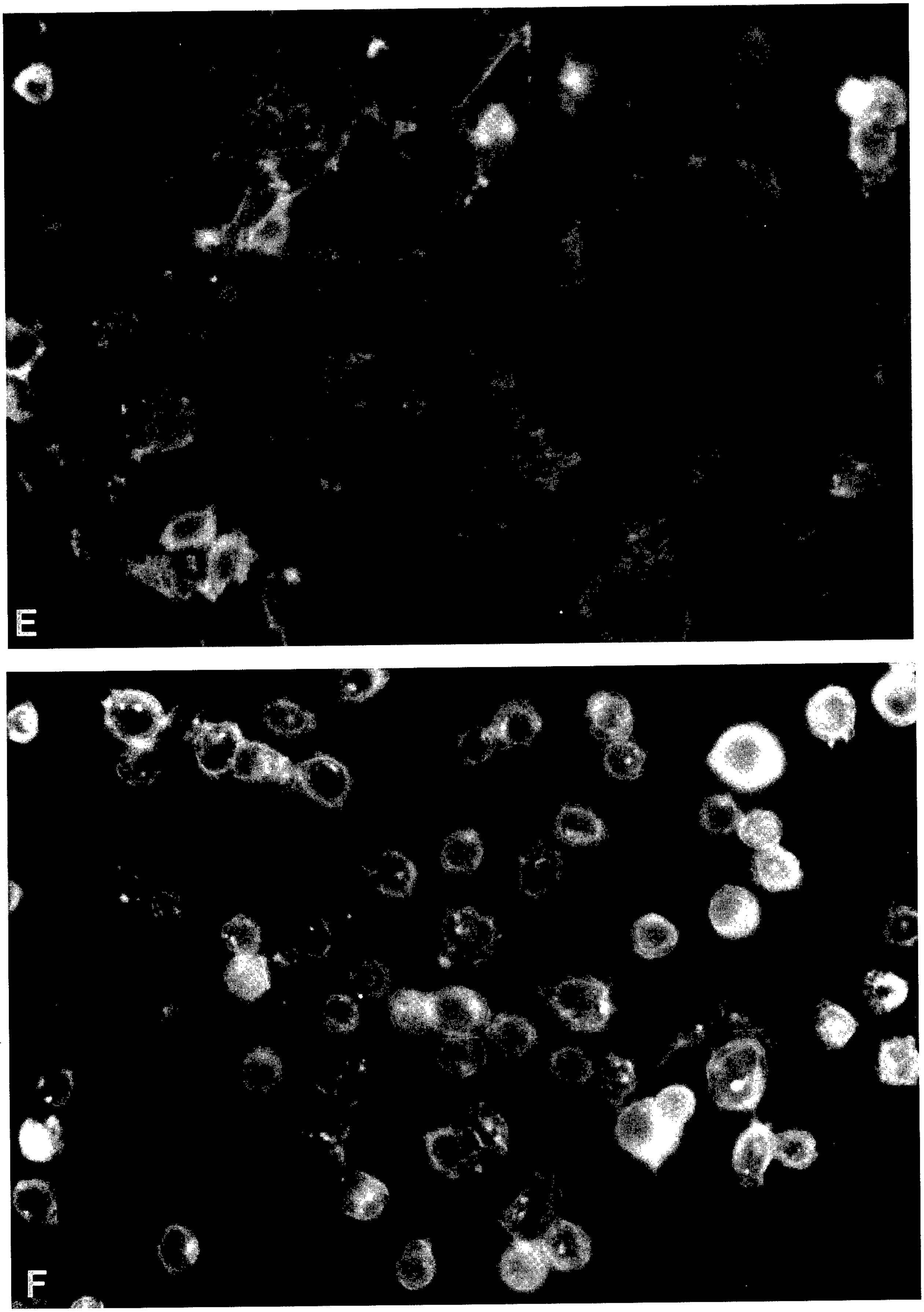

FIG. 6—*Continued*

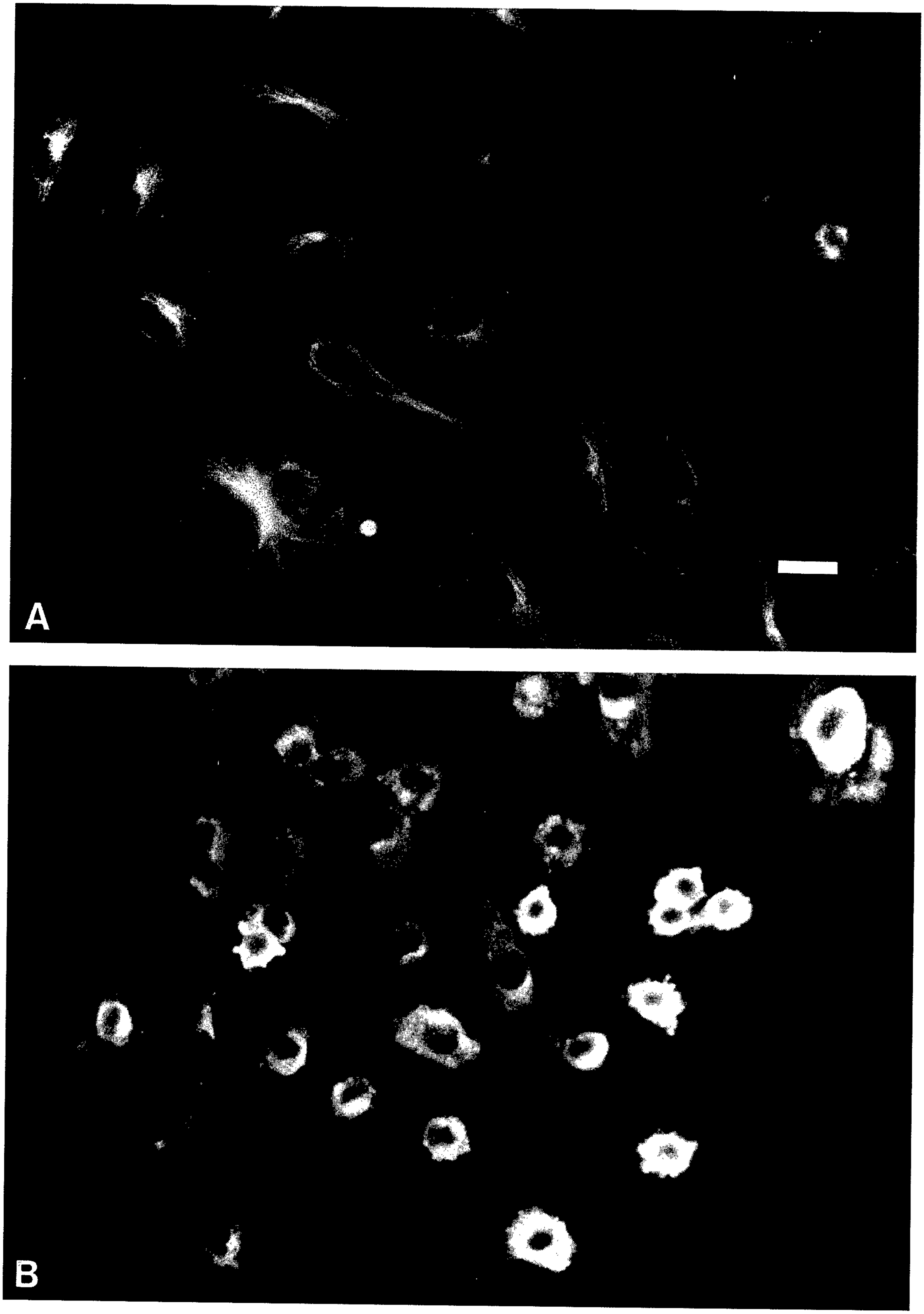
A
B

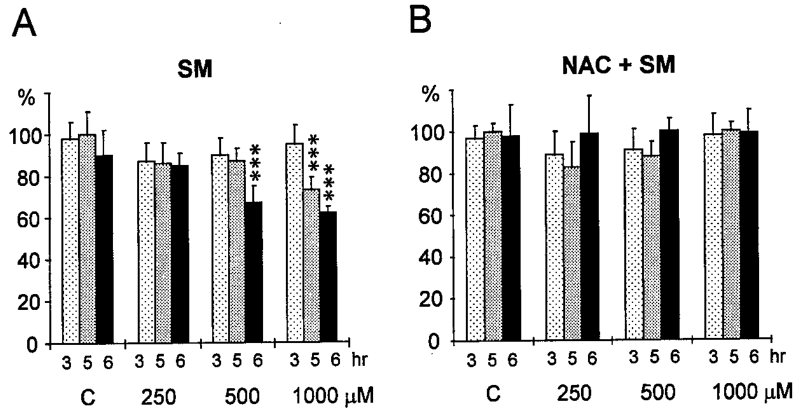

FIG. 8. Number of adherent endothelial cells present during the time course of SM injury, without (A) and with (B) NAC pretreatment. At each experimental time point the media were removed and cells were harvested by incubation with 0.05% trypsin and 0.02% EDTA for 1 min and washed with the medium. Then, the cell suspension was counted using an hemocytometer. The data are shown as a percentage of cell number at Time 0. $^{***}p \leqslant 0.006$ (SM versus control).

shaw *et al.,* 1991). The rate and extent of actin polymerization appear to correlate with the degree of sulfhydryl oxidation occurring in the injured cells. DNase I measurement of monomeric G-actin as a percentage of total actin suggests an early trend toward actin assembly (decrease in G-actin as a percentage of total actin) at 1000 μM SM and a later trend toward actin depolymerization (increase in G-actin) at the same concentration. Since a smaller portion of the total population of adherent cells at any given time point is apoptotic, the changes in actin measurable with the DNase I assay represent an average of the whole population of cells. Thus it is not surprising that only at 1000 μM SM changes in (G)-actin content were significant, since at this concentration of the agent the greatest number of cells was dying in a synchronized manner. From the fluorescence microscopic examination of microfilaments containing F-actin we hypothesize that actin depolymerization also occurs in endothelial cells exposed to lower concentrations of SM.

While rounding was observed among both apoptotic and necrotic cells, microfilament reorganization proceeded differently, depending on the dominant pattern of cell death. In necrotic cells it was accompanied by a total disruption of microfilaments, whereas in apoptotic cells only disruption of long actin filament stress fibers was observed while the cortical band of actin remained intact but decreased in diameter. Stress fibers which are sensitive to ATP depletion (Sanger *et al.,* 1983) are thought to play a role in cellular adhesion (Gottlieb *et al.,* 1991; White, 1983), while the cortical band of actin may represent the most dynamic component of the cytoskeleton, involved in retraction of cellular processes (Lawson, 1987). The SM-induced appearance of floating cells (among which necrotic cells were predominant) correlated well with rapid and significant depletion of intracellular ATP and loss of stress fiber architecture. The constricted cortical band of actin in apoptotic cells may be essential for the gradual shrinkage of cells observed during apoptosis. Microtubule depolymerization was seen in cells injured by high concentrations of SM and may take place when either an injury is sufficiently severe to cause loss of intracellular Ca^{2+} homeostasis or there is a sustained elevation of intracellular Ca^{2+} for other reasons (Hinshaw *et al.,* 1989).

Pathophysiological Relevance of SM-Induced Cytoskeletal Reorganization

Actin associated proteins play structural and/or regulatory roles in the organization of microfilaments (Button *et al.,* 1995). It is possible, that several of these proteins may be affected by modification of their sulfhydryl groups via direct reaction with SM or with endogenously produced reactive oxygen species (Papirmeister *et al.,* 1991). Cleavage of fodrin, a protein which cross-links actin filaments at their ends and associates with the plasma membrane (Harris and Morrow, 1990) is tightly coupled to apoptosis (Martin, 1995). In our experiments, we found that NAC pretreatment alone (without SM injury) induced a rearrangement of actin filaments. Modification of the cellular redox status by NAC

FIG. 7. Microtubules in endothelial cells visualized by fluorescence microscopy, fixation, and staining as described under Materials and Methods. (A) Control cells; (B) cells exposed to 1000 μM SM at 5-hr time point. Microtubule depolymerization was also seen to a lesser extent after injury with 500 μM SM (data not shown). Bar is equivalent to 20 μm.

pretreatment may alter the association of actin binding proteins involved in apoptosis (e.g., fodrin) with actin filaments. NAC-induced changes in their association with actin filaments may alter visible microfilament organization as well as susceptibility to signaling events involved in apoptosis induction (e.g., fodrin cleavage).

Cell rounding, contraction, and gap formation observed after SM injury is accompanied by an increase in endothelial paracellular transport (Lum and Malik, 1994). In our study NAC pretreatment totally prevented cell rounding following injury with lower doses (250 μM) of SM and partially prevented this phenomenon even at higher (≥500 μM) concentrations of SM. NAC pretreatment could modify some cytoskeletal component(s) responsible for cell-to-cell and cell-substrate adhesion (Kupffer *et al.,* 1983). Using a model permeability barrier composed of confluent monolayers of endothelial cells we also found (unpublished observations) that exposure to 250 μM SM increased albumin transport across the endothelial cell barrier two- to threefold over the control rate of flux. Pretreatment with NAC reduced the amount of albumin flux to 1.5× that of the control which further supports the concept that enhanced cellular adherence and stress fiber architecture induced by NAC pretreatment may have relevance to understanding endothelial cell dysfunction following SM injury.

High concentrations of SM (≥500 μM) induced loss of endothelial cell adherence, which was observed by the appearance of floating cells. Actin stress fibers are linked to the extracellular matrix through integrin receptors and focal adhesions (Nobes and Hall, 1995). Although loss of adherence may be an important element in the induction of apoptosis in some models (Ruoslathi and Reed, 1994), major features of apoptosis (DNA "ladders," membrane budding, and apoptotic body formation) developed predominantly in adherent cells after SM exposure in this study. The protective effect of NAC pretreatment in preventing apoptosis may be more related to its effect on microfilament stress fiber architecture than its collateral effects on cellular adhesion. The fact that NAC pretreatment completely prevented the loss of cellular adherence even at 1000 μM SM, a concentration at which a high percentage of necrotic cells was present, indicates that at least in this model of injury loss of cellular adherence is not a simple consequence of cell death. Our data are consistent with other work demonstrating NAC-enhanced adhesion properties of epithelial and lymphoid cells (Rivabene *et al.,* 1995).

In conclusion, SM induced both apoptotic and necrotic forms of cell death in endothelial cells. Disruption of the long actin filament stress fibers and rounding of cells preceded other features of apoptosis. Pretreatment with NAC clearly influenced cytoskeletal organization and nearly eliminated all apoptotic features of cell death but did not prevent necrosis in response to SM. Based on these observations, it is likely that actin filament organization together with cell substratum adhesion may be important elements in determining cellular susceptibility to apoptotic stimuli. Since NAC pretreatment can inhibit the SM-induced apoptotic pathway of endothelial cell death it may also have important implications for treatment of the vascular lesions induced by SM.

REFERENCES

Arends, M. J., and Wyllie, A. H. (1991). Apoptosis: Mechanisms and roles in pathology. *Int. Rev. Exp. Pathol.* **32,** 223–254.

Burgunder, J. M., Varriale, A., and Lauterburg, B. H. (1989). Effect of N-acetylcysteine on plasma cysteine and glutathione following paracetamol administration. *Eur. J. Clin. Pharmacol.* **36,** 127–131.

Bursch, W. (1990). The biochemistry of cell death by apoptosis. *Biochem. Cell. Biol.* **68,** 1071–1074.

Button, E., *et al.* (1995). Actin, its associated proteins and metastasis. *Cell Motil. Cytoskel.* **30,** 247–251.

Cohen, J. J. (1991). Programmed cell death in the immune system. *Adv. Immunol.* **50,** 55–85.

Cowan, F. M., *et al.* (1992). Inhibition of sulfur mustard increased protease activity by niacinamide, N-acetyl-L-cysteine or dexamethasone. *Cell. Biol. Toxicol.* **8**(2), 129–138.

Dannenberg, A. M., Jr., *et al.* (1985). Inflammatory mediators and modulators released in organ-culture from rabbit skin lesions produced in vivo by sulfur mustard. I. Quantitative histopathology; PMN, basophil and mononuclear cell survival; and unbound (serum) protein content. *Am. J. Pathol.* **121,** 15–27.

De Flora, S., and De Vries, N. (1993). N-acetyl-cysteine. *J. Cell. Biochem.* (Suppl.) **17,** 270–277.

Duke, R. C., and Cohen, J. J. (1992). Morphological and biochemical assays of apoptosis. *Curr. Prot. Immunol.* (Suppl. 3) **17,** 1–16.

Friedenwald, J. S., and Buschke, W. (1948). Nuclear fragmentation produced by mustard and nitrogen mustards in the corneal epithelium. *Bull. Johns Hopkins Hosp.* **82,** 161–177.

Ginzler, A. M., and Davis, M. I. J. (1943). The pathology of mustard burns of human skin. U.S. Army Medical Research Laboratory, Edgewood Arsenal, MD, Rep. No. 3.

Gottlieb, A. I., *et al.* (1991). Biology of disease. Structure and function of the endothelium cytoskeleton. *Lab. Invest.* **65,** 123–137.

Gross, C. L., *et al.* (1993 Jul–Sep). Biochemical manipulation of intracellular glutathione levels influences cytotoxicity to isolated human lymphocytes by sulfur mustard. *Cell. Biol. Toxicol.* **9**(3), 259–267.

Haake, A. R., and Polakowska, R. R. (1993). Cell death by apoptosis in epidermal biology. *J. Invest. Dermatol.* **101**(2), 107–112.

Harris, A. S., and Morrow, J. S. (1990). Calmodulin and calcium-dependent protease I coordinately regulate the interaction of fodrin with actin. *Proc. Natl. Acad. Sci. USA* **87,** 3009–3013.

Hinshaw, D. B., *et al.* (1993). ATP depletion induces an increase in the assembly of a labile pool of polymerized actin in endothelial cells. *Am. J. Physiol.* **264,** C1171–C1179.

Hinshaw, D. B., *et al.* (1991). Actin polymerization in cellular oxidant injury. *Arch. Biochem. Biophys.* **288,** 311–316.

Hinshaw, D. B., *et al.* (1986). Cytoskeletal and morphological impact of cellular oxidant injury. *Am. J. Pathol.* **123,** 454–464.

Hinshaw, D. B., *et al.* (1989). Mechanism of endothelial cell shape change in oxidant injury. *J. Surg. Res.* **46,** 339–349.

Hockenbery, D. (1995). Defining apoptosis. *Am. J. Pathol.* **146,** 16–19.

Hockenbery, D. M., *et al.* (1993). Bcl-2 functions in an antioxidant pathway to prevent apoptosis. *Cell* **75,** 241–251.

Kane, D. J., *et al.* (1993). Bcl-2 inhibition of neural death: Decreased generation of reactive oxygen species. *Science* **262,** 1274–1277.

Kupffer, A., *et al.* (1983). Polarization of the golgi apparatus and the microtubule organizing center within cloned natural killer cells bound to their targets. *Proc. Natl. Acad. Sci. USA* **80,** 7224–7228.

Laird, P. W., *et al.* (1991). Simplified mammalian DNA isolation procedure. *Nucleic Acids Res.* **19,** 4293.

Lawson, D. (1987). Distribution of myosin and relationship to actin organization in cortical and subcortical areas of antibody-labelled, quick-frozen, deep-etched fibroblast cytoskeletons. *Cell Motil. Cytoskel.* **7,** 368–380.

Lum, H., and Malik, A. B. (1994). Regulation of vascular endothelial barrier function. *Am. J. Physiol.* **267,** L223–L241.

Majno, G., and Joris, I. (1995). Apoptosis, oncosis, and necrosis. An overview of cell death. *Am. J. Pathol.* **146,** 3–15.

Malorni, W., *et al.* (1993). N-acetylcysteine inhibits apoptosis and decreases viral particles in HIV chronically infected U937 cells. *FEBS Lett.* **327,** 75–78.

Martikainen, P., Kyprianou, N., and Isaacs, J. T. (1990). Effect of transforming growth factor β-1 on proliferation and death of rat prostatic cells. *Endocrinology* **127,** 2963–2968.

Martin, S. J. (1995). Proteolysis of fodrin (non-erythroid spectrin) during apoptosis. *J. Biol. Chem.* **270,** 6425–6428.

Meier, H. L., Gross, C. L., and Papirmeister, B. (1987). 2,2-Dichlorodiethyl sulfide (sulfur mustard) decreases NAD^+ levels in human leukocytes. *Toxicol. Lett.* **39,** 109–122.

Meister, A., Anderson, M. E., and Hwang, O. (1986). Intracellular cysteine and glutathione delivery systems. *J. Am. Coll. Nutr.* **5,** 137–151.

Mitcheltree, L. W., *et al.* (1989). Microblister formation in vesicant-exposed pig skin. *J. Toxicol. Cut. Ocul. Toxicol.* **8,** 309–319.

Mol, M. A. E., Van deRuit, A.-M. B. C., and Kluivers, A. W. (1989). NAD+ levels and glucose uptake of cultured human epidermal cels exposed to sulfur mustard. *Toxicol. Appl. Pharmacol.* **98,** 159–165.

Mol, M. A. E., *et al.* (1991). Effects of nicotinamide on biochemical changes and microblistering induced by sulfur mustard in human skin organ cultures. *Toxicol. Appl. Pharmacol.* **107,** 439–449.

Momeni, A., Enshaeih, S., and Meghdadi, M. (1992). Skin manifestations of mustard gas. *Arch. Dermatol.* **128,** 775–779.

Nobes, C. D., and Hall, A. (1995). Rho, rac and cdc42 GTPases; regulators of actin structures, cell adhesion and motility. *Biochem. Soc. Trans.* **23**(3), 456–459.

Papirmeister, B., *et al.* (1991). Medical defense against mustard gas: Toxic mechanisms and pharmacological implications. CRC Press, Boca Raton, FL.

Papirmeister, B., *et al.* (1985). Molecular basis for mustard-induced vesication. *Fund. Appl. Toxicol.* **5,** S134–S149.

Reed, J. (1994). Bcl-2 and the regulation of programmed cell death. *J. Cell Biol.* **124,** 1–6.

Rikimaru, T., *et al.* (1991). Mediators, initiating the inflammatory response, released in organ culture by full-thickness human skin explants exposed to the irritant, sulfur mustard. *J. Invest. Dermatol.* **96**(6), 888–897.

Rivabene, R., *et al.* (1995). N-acetyl-L-cysteine enhances cell adhesion properties of epithelial and lymphoid cells. *Cell Biology International* **19**(8), 681–686.

Ruoslathi, E., and Reed, J. C. (1994). Anchorage dependence, integrins, and apoptosis. *Cell* **77,** 477–478.

Sanger, J. W., *et al.* (1983). Differential response of three types of actin filament bundles to depletion of cellular ATP levels. *Eur. J. Cell Biol.* **31**(2), 197–204.

Schwartzman, R. A., and Cidlowski, J. A. (1993). Apoptosis: The biochemistry and molecular biology of programmed cell death. *Endocrinol. Rev.* **14,** 133–151.

Smith, K. J., *et al.* (1995). Sulfur mustard: Its continuing threat as a chemical warfare agent, the cutaneous lesions induced, progress in understanding its mechanism of action, its long-term health effects, and new developments for protection and therapy. *J. Am. Acad. Dermatol.* **32,** 765–776.

Vaughan, F. L., *et al.* (1988). Macromolecular metabolism of a differentiated rat keratinocyte culture system following exposure to sulfur mustard. *J. Toxicol. Environ. Health* **23,** 507–518.

White, G. E. (1983). Factors influencing the expression of stress fibers in vascular endothelial cells in situ. *J. Cell Biol.* **97,** 416–424.

Willems, J. L. (1989). Clinical management of mustard gas casualties. *Ann. Med. Milit. Belg.* **3,** 1–61.

Wulf, E., *et al.* (1979). Fluorescent phallotoxin, a tool for the visualization of cellular actin. *Proc. Natl. Acad. Sci. USA* **76,** 4498–4502.

Yourick, J. J., *et al.* (1991). Niacinamide pretreatment reduces microvesicle formation in hairless guinea pigs cutaneously exposed to sulfur mustard. *Fund. Appl. Toxicol.* **17**(3), 533–542.

Zhang, Z., *et al.* (1995). Evaluation of protective effects of sodium thiosulfate, cysteine, niacinamide and indomethacin on sulfur mustard-treated isolated perfused porcine skin. *Chem. Biol. Interact.* **96**(3), 249–262.

Zhong, L. T., *et al.* (1993). Bcl-2 inhibits death of central neural cells induced by multiple agents. *Proc. Natl. Acad. Sci. USA* **90**(10), 4533–4537.